D17-2024-16

Yu. M. Shukrinov [1,2,*], A. E. Botha [3,**]

JINR-UNISA RESULTS OF COLLABORATION ON THEORETICAL STUDY OF JOSEPHSON NANOSTRUCTURES

Submitted to "Physics of Particles and Nuclei"

[1] Joint Institute for Nuclear Research, Dubna
[2] Dubna State University, Dubna
[3] University of South Africa, Johannesburg, South Africa
[*] E-mail: shukrinv@theor.jinr.ru
[**] E-mail: bothaae@unisa.ac.za

Шукринов Ю. М., Бота А. Е. Д17-2024-16

Результаты сотрудничества ОИЯИ-UNISA в области
теоретических исследований джозефсоновских наноструктур

Представлен обзор результатов, полученных в рамках сотрудничества ОИЯИ–UNISA в области теоретического исследования джозефсоновских наноструктур. В частности, наша работа включала исследование широкого спектра нелинейных динамических эффектов различных систем джозефсоновских переходов, в частности системы внутренних джозефсоновских переходов в высокотемпературных сверхпроводниках и переходы сверхпроводник/ферромагнетик/сверхпроводник, которые в настоящее время интенсивно исследуются в связи с их применением в сверхпроводниковой электронике и спинтронике.

Работа выполнена в Лаборатории теоретической физики им. Н. Н. Боголюбова ОИЯИ.

Препринт Объединенного института ядерных исследований. Дубна, 2024

Shukrinov Yu. M., Botha A. E. D17-2024-16

JINR-UNISA Results of Collaboration
on Theoretical Study of Josephson Nanostructures

An overview of the results obtained within the framework of the JINR–UNISA collaboration in the field of theoretical study of Josephson nanostructures is presented. In particular, our work has involved studies of a wide variety of nonlinear dynamic effects in various systems of coupled Josephson junctions, including superconductor/ferromagnet/superconductor junctions, which are currently being investigated intensively due to the potential applications in superconducting electronics and spintronics.

The investigation has been performed at the Bogoliubov Laboratory of Theoretical Physics, JINR.

Preprint of the Joint Institute for Nuclear Research. Dubna, 2024

INTRODUCTION

Collaboration between the Joint Institute for Nuclear Research (JINR) and the University of South Africa (UNISA) in the field of theoretical studies of superconducting nanostructures started with the discussions held at the 56th Annual Conference of the South African Institute of Physics (SAIP), from 12–15 July 2011. At this conference, which was hosted by UNISA, A. E. B. presented computer simulations of optimized periodic and hyperchaotic modes in a triple pendulum system [1] and Yu. M. S. presented a talk on parametric resonance features in the coupled Josephson junctions [2]. Because the single, damped, driven pendulum is a well-known mechanical analogy of the Josephsnon junction, these computer simulations drew the attention of Yu. M. S., who was also participating in the conference to present simulations of intrinsic Josephson junctions. During the subsequent discussions, we realized that the two systems in fact share a number of similarities. Mathematically, both are composed of the same basic entity, differing only in the way they are coupled together. Thus, the fact that very similar simulation and analytic techniques could be applied profitably to both systems formed the basis of our collaboration.

Prior to the 56th Annual Conference of the SAIP, and largely due to the efforts of the late Professors S. A. Sofianos (UNISA) and V. B. Belyaev (JINR), the foundations for collaboration between the two institutions had been firmly cemented [**?**]. The first DST-UNISA–JINR Symposium was organized at Skukuza, in the Kruger National Park, during February of 2007 (see Fig. 1), and the second South Africa – JINR Symposium was held in Dubna, during September of 2010 (see Fig. 2).

Both symposiums helped to establish a fruitful and ongoing collaboration between the two (predominantly nuclear/particle) physics communities. However, by the time of the third Symposium, which was held in Stellenbosch during November of 2012, several new areas of scientific cooperation had also been established. At the third symposium, we presented our first collaborative research on resonance-related chaos in certain systems of intrinsic Josephson junctions [3]. Since then, our research has encompassed the investigation of many different dynamical effects related to the Josephson junction structures, including the occurrence of breathing chimera states in intrinsically coupled Josephson junctions [4, 5] and simulations revealing a signature for the possible experimental detection of the Majorana fermions in superconducting quantum interference devices (SQUIDs), with nontrivial barriers [6].

Fig. 1. Sitting on their haunches, from left to right, are: D. V. Kamanin (JINR Deputy Chief Scientific Secretary) and Professor S. A. Sofianos (Department of Physics, UNISA). Fourth from the left (standing) is Dr. Rob Adam, who was at that time the Director General of the Department of Science and Technology (DST) in South Africa

Fig. 2. Some of the participants standing outside the BLTP building on the occasion of the 2nd SA–JINR Symposium "Models and Methods in Few- and Many-Body Systems", 8–10 September 2010, Dubna, Russia

Recently, in an effort to further extend the scope of the SA–JINR collaboration, a new series of workshops was started. In January of 2020, we participated in the first South Africa–JINR workshop on theory and computation (see Fig. 3). Due to the drawn-out COVID-19 pandemic that reached South Africa in March of the same year, the second workshop was delayed until December of 2023. However, we anticipate that this new series of workshops will continue at more regular intervals in the future, and that they will assist in strengthening future collaborations. To date, our own collaboration has produced 26 journal articles [3, 5, 7–25, 27–31], 11 conference proceedings [1, 4, 6, 26, 32–38] and many conference abstracts, e.g., [39–43].

In what follows we will provide a comprehensive overview of our collaborative research during the past twelve years. The order in which it is described under the following section headings is more or less chronological. In Section 1, we discuss the emergence of chaos in a system of coupled (intrinsic) junctions, caused by the parametric resonance. Section 2 introduces the idea of structured chaos that we discovered in a single Josephson junction under the influence of external electromagnetic radiation. Section 3 continues with our analysis of the single, driven junction by demonstrating the existence of a Farey staircase, resulting from the two-extremum (as opposed

Fig. 3. The first SA–JINR workshop on theory and computation held on 27–29 January 2020 near the beautiful town of Franschhoek — Western Cape wine lands

to unimodal) return map of the junction. In Section 4, we return to the intrinsic junctions and show that they are capable of exhibiting spontaneous and controlled chaos synchronization, in response to externally applied electromagnetic radiation. We found and first described the spontaneous and controlled chaos synchronization in intrinsic Josephson junctions, a property that is useful for chaos encryption. Section 5, discusses chaos that occurs along the resonance circuit branch of a system of intrinsic Josephson junctions shunted by resistive (R), inductive (L) and capacitive (C) elements. Here the dynamics is complicated by the fact that the frequency of the RLC resonance circuit couples to the oscillations of the intrinsic junctions, which have their own current-dependent natural frequency. Section 6 shows specific ladder structures that appear in the superconductor–ferromagnetic–superconductor (S–F–S) Josephson junction under the action of a circularly polarized magnetic field. In these S–F–S structures, the chaotic and bifurcation features are obviously important for the develpoment of reliable superconductor electronic devices, as discussed in Section 7. Hysteresis and chaos in anomalous Josephson junctions without capacitance, i.e., underdamped, are discussed in Section 8. Here we see that there is multistability due to the coupling with the magnetic moment. Such multistability is crucial to applications that involve switching, e.g., memory devices.

In Section 9, we have analyzed the bifurcation structure and chaos that occurs in a nanomagnet, coupled to a Josephson junction. Here the coupling is through the magnetic vector potential, rather than being intrinsic. In our studies discussed in Section 10, we were able to show that, over a considerable range of coupling strengths, a model of the intrinsic Josephson junctions with a more extended coupling range could support the occurrence of the so-called breathing chimeric states. In Section 11, we discuss how our results on the resonance phenomena that occurs in high-T_c superconductors allowed us to propose a novel method for the determination of charging the superconducting layers, based on the voltage dynamics. Charging of the superconducting layers in shunted high T_c superconductors is discussed in Section 12. A full magnetization reversal in an S–F–S structure with spin-orbit coupling, via the application of an optimized electric current pulse was demonstrated in the work discussed in Section 13. Such a reversal may be important for certain applications in quantum computing.

In Section 14, we show that the φ_0 junction possesses rich variety of dynamical states determined by both the parameters of the Josephson junction and those of the intermediate ferromagnetic layer. Interestingly, it shows features reminiscent of the famous Kapitza pendulum. In Section 15, we investigate the effects of the ferromagnetic resonance and magnetization dynamics on the current–voltage characteristics (CVCs) of the S–F–S φ_0 junction. This leads to a "kink" structure in the CVCs. Then, in Sections 16 and 17, we shift our attention to a related model, know as the Frenkel–Kontorova (F–K) model. We study first the overdamped case (Section 16) and then the underdamped case (Section 17). The F–K model is important because of its generality and the fact that it shares many feastures

with various models of Josephson junctions. It is often used as a model to study tribology (friction) in various systems. In Section 18, we explain the relevance of Josephson junctions to the important real-world problem of achieving synchronicity in electrical power distribution grids. In the final section we provide a conclusion and outlook towards future collaboration on some of the potential applications that our more recent work could have on the revelopment of superconducting electronic and spintronic devices.

1. CHAOS AND RESONANCES IN COUPLED JOSEPHSON JUNCTIONS

Based on our collaboration we have created a significant groundwork for the investigation and modeling of chaotic phenomena in a system of coupled Josephson junctions [3, 5, 7–10, 32]. In particular, the emergence of chaos in a system of coupled junctions, caused by parametric resonance, as well as structured chaos under the influence of external electromagnetic radiation has been demonstrated. We have found that in a stack of intrinsic Josephson junctions the chaotic features are triggered by the coupling between different junctions in the stack. Spontaneous and controlled chaos synchronization in intrinsic Josephson junctions were described. Chaotic and bifurcation features that are important for superconducting electronics were demonstrated in superconductor–ferromagnet–superconductor nanostructures. Below we present some of our collaborative results in this area.

Chaotic features of the systems of coupled Josephson junctions were studied in [3]. Manifestation of chaos in the temporal dependence of the electric charge, related to a parametric resonance, was demonstrated through the calculation of the maximal Lyapunov exponent, phase–charge and charge–charge Lissajous diagrams and correlation functions. We have shown that a number of junctions in the stack strongly influences the fine structure in the current–voltage characteristics and a strong proximity effect results from the nonperiodic boundary conditions. The observed resonance-related chaos exhibits intermittency over a range of conditions and parameters. General features of the system were analyzed by means of a linearized equation and the criteria for a break point region (BPR) with no chaos were obtained. Such criteria clarified experimental observations of variations in the power output from intrinsic Josephson junctions in high-temperature superconductors [44].

Figure 4 (top) shows the maximal Lyapunov exponent (blue line) as a function of the bias current and the upper-most branch of the current–voltage characteristic (red line) in comparison with the time dependence of the electric charge at the 8th JJ (green). The inset shows the position of the break point on the upper branch of the current–voltage characteristic. Both the current–voltage characteristic and the time dependence of the charge demonstrate chaotic behavior in the current range in which $\mathrm{LE} > 0$.

The study of correlations between the superconducting currents in neighboring intrinsic Josephson junctions allowed us to explain some of the chaotic features observed in the current–voltage characteristics (CVC).

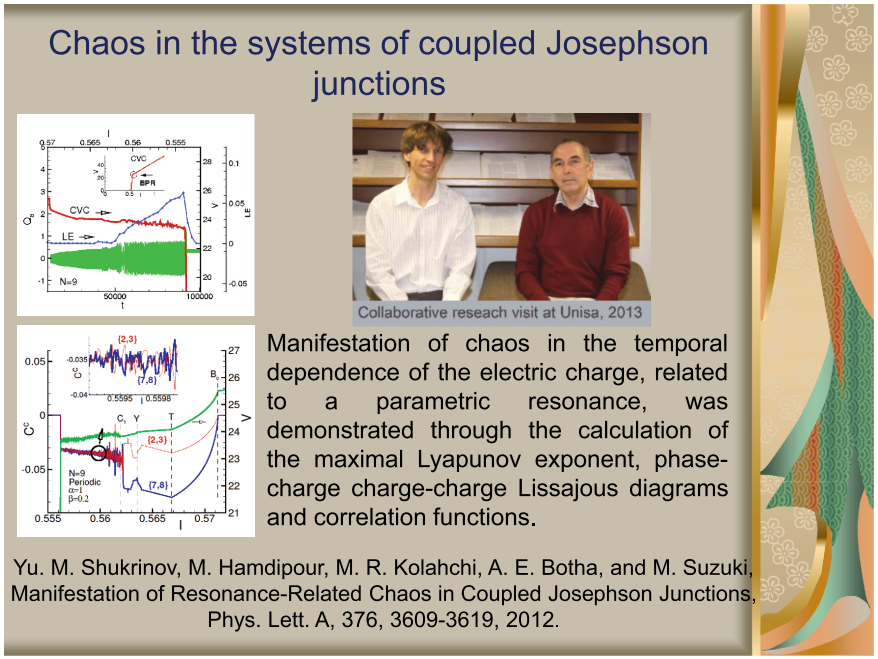

Fig. 4. Top: Lyapunov exponent as a function of bias current and current–voltage characteristics together with the time dependence of the charge on the 8th superconducting layer Q_8. The insert shows the position of the break point on the upper branch of the current–voltage characteristic. Bottom: the charge correlation functions $C^c_{l,l+1} = \langle Q_l(t)Q_{l+1}(t)\rangle$ for $l = 2$ (labeled by *2*, *3*) and $l = 7$ (labeled *7*, *8*) for the stack with nine IJJ as a function of the bias current. Adapted from [3]

The lower result, towards the left of Fig. 4, is from a calculation of the correlations between the $l = 2$ and $l = 7$ junctions, within a stack of nine intrinsic junctions. Based on these results, the expected feature of the correlation functions in the chaotic region was confirmed: *at the transition to chaotic behavior (point C_1), the values of all correlation functions approach each other, i.e., $\langle Q_l(t)Q_{l+1}(t)\rangle = \langle Q_l(t)\rangle \langle Q_{l+1}(t)\rangle$. Thus, within the chaotic region, all correlations are lost.*

We have also demonstrated, for the first time, that intermittency can occur as a result of resonance related chaos in systems of coupled JJs. Many such transitions can be seen in Fig. 5, *a*, where we present results of a high precision calculation of the largest Lyapunov exponent (LE) together with the CVC, for a stack of nine junctions, using nonperiodic boundary conditions, at $\gamma = 0.5$.

To gain more information about the transitions we investigate the dependence of all the charge–charge correlation functions (CCF) and the LE, on the bias current in the BPR. As the LE shows, in Fig. 5, *b*, the absence

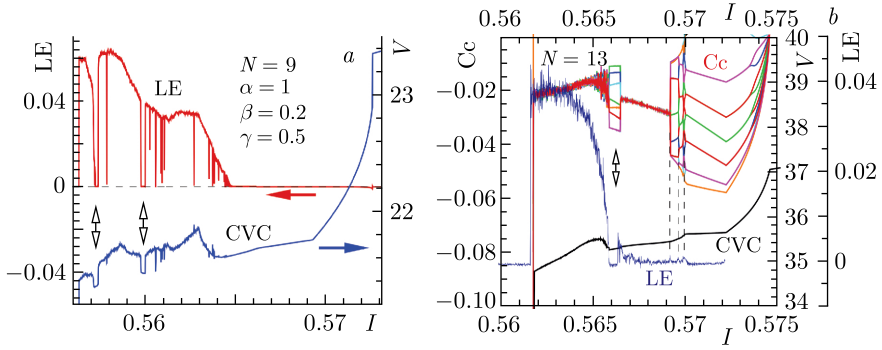

Fig. 5. *a*) Intermittency is shown by windows of LE = 0 inside the chaotic dynamics. Arrows point to the respective scales for each curve and the dashed line shows the LE = 0 axis. Double arrows show the correspondence between features of the CVC and the LE. *b*) Demonstration of the intermittency within the interval of bias current $0.5659 < I < 0.5565$ (shown by a double arrow) for the charge–charge correlation functions (Cc) and LE for a periodic stack of 13 junctions. Adapted from [3]

of the charge correlations in different S-layers is a signature of the chaotic behavior. We see a restoration of correlations in the middle of the chaotic region for a stack with 13 JJs. All presented characteristics (CCF, CVC and LE) reflect this transition from the chaotic behavior to regular and back. Our results stress the agreement between the correlation functions and LE.

2. STRUCTURED CHAOS AND THE DEVIL'S STAIRCASE IN A DRIVEN JOSEPHSON JUNCTION

In [7] the detailed numerical simulations of the CVC of a Josephson junction under external electromagnetic radiation show the devil's staircase within different bias current intervals. We have found that the observed steps form very precisely continued fractions. Increase of the amplitude of the radiation shifts the devil's staircase to higher Shapiro steps. An algorithm for the appearance and detection of subharmonics with increasing radiation amplitude is proposed.

The steps in the ladder structure form continuous fractions of voltage and are determined with

$$V = \left(N \pm \cfrac{1}{n \pm \cfrac{1}{m \pm \cfrac{1}{p \pm \dots}}} \right) \omega, \qquad (1)$$

where $N, n, m, p, \dots$ are positive integers. By reducing eq. (1) by N, one can obtain the conditions of the first level of the continued fraction, corresponding

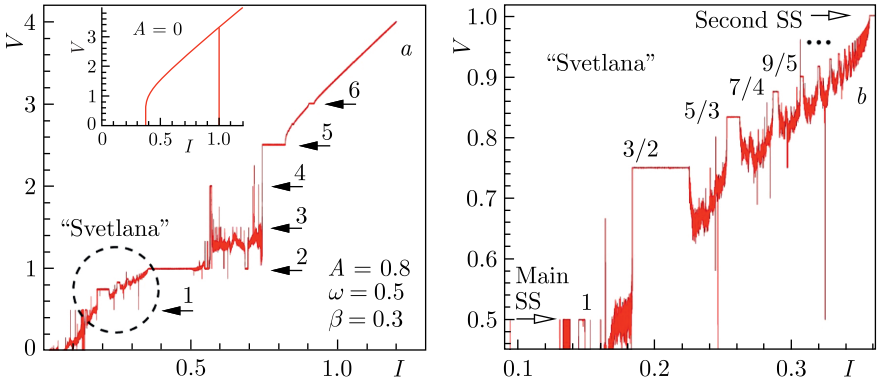

Fig. 6. *a*) I–V characteristics of the JJ at $\beta = 0.3$, $\omega = 0.5$ and $A = 0.8$. The arrows indicate the harmonic number of the Shapiro step. The inset shows the current–voltage characteristic without radiation. *b*) Enlarged part of the current–voltage characteristic ("Svetlana" structure) circled in (*a*), showing steps alternating with chaotic regions. Adapted from [10]

to the main Shapiro step, or harmonics. Similarly, by reducing the formula by n, we can obtain second-level conditions that correspond to subharmonics of the Shapiro steps. We showed that the experimental results are easy to classify based on our continued fraction formula. We have demonstrated that the subharmonic steps registered in the well-known experiments by Dayem and Wiegand [Phys. Rev. 155, 419 (1967)] and Clarke [Phys. Rev. B 4, 2963 (1971)] also form continued fractions.

In [10] it was found that the subharmonic Shapiro steps at certain parameters are separated by structured chaotic windows which exhibit scaling similarity. This structure in I-V characteristic was called "Svetlana". The onset of chaos for subharmonic steps occurs through the Feigenbaum period doubling scenario. Universality in the sequence of periodic windows (U-sequence) was also demonstrated and concluded that the structured chaos is a stable formation over a wide range of parameter values. The current–voltage characteristic of the JJ at $\omega = 0.5$ and $A = 0.8$ is shown in the main part of Fig. 6, *a*.

An enlarged part of the current–voltage characteristic region marked with a circle in Fig. 6, *a* is presented in Fig. 6, *b*. In this region, the current–voltage characteristic shows alternating stable and chaotic regions, i.e., structured chaos.

3. FAREY STAIRCASE FROM THE TWO-EXTREMUM RETURN MAP OF A JJ

We report new synchronization phenomena occurring over a relatively small region of previously unexplored parameter space in the RCSJ model of a single Josephson junction under external electromagnetic radiation. Two

identical Farey staircases, one displaced relative to the other, are observed in the current–voltage characteristics of the junction. As the current (dissipation parameter) of the system is increased (decreased), the two staircases merge into one staircase. The existence of the Farey staircase itself can be understood in terms of a one-dimensional iterative map which contains two extrema, and the displacement of the two staircases is related to folding (double-valuedness) in the return map, reflecting the higher fractional dimensionality of the system.

In Fig. 7, we show manifestations of Farey staircases in the CVC at various amplitudes A. The subharmonics seen here all occur between the second ($V = 1$) and third ($V = 1.5$) harmonics. The inset to the figure shows an enlarged view of the CVC at $A = 0.1$.

There are also chaotic intervals present between the two staircases, without the staircase having ever been complete. This suggests that Chirikov's resonance overlap scenario [60] may apply, even though the universal quasiperiodic route to chaos is not followed. At higher currents, the Farey staircase eventually joins the third harmonic, after an infinite number of steps. At the bifurcation point, between the last step and the lower (in current) edge of the third harmonic the system exhibits an instance of the bifurcation known as blue-sky catastrophe [42]. This is the first such instance to be reported in the RCSJ model. The sinusoidal coupling in the model makes it distinct from other low order models that can exhibit BSC. In other

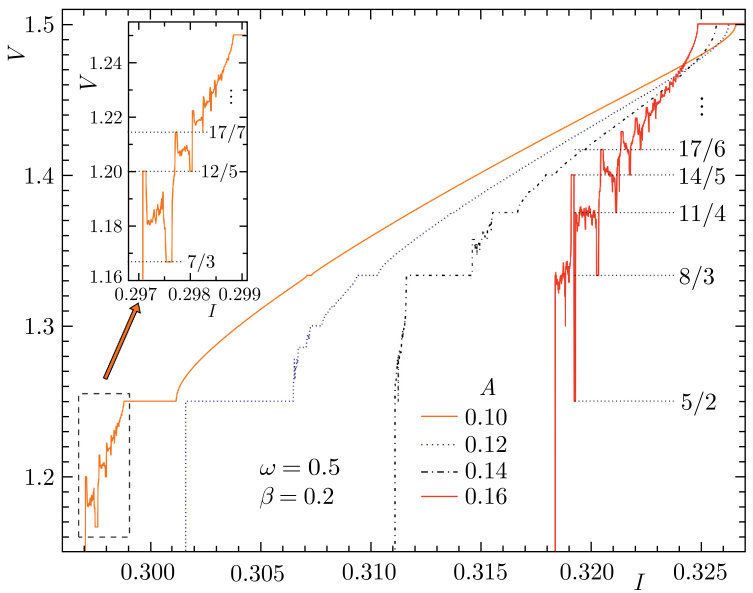

Fig. 7. Farey staircases in the CVC at four different amplitudes A. Here V denotes the time-averaged voltage. Adapted from [15]

models of BSC, there are quadratic [61] or cubic [44] response functions. The details of the time series in voltage, as the staircase is ascended and third harmonic is approached, show resemblances to the bursting phenomena observed in a neuron model [43, 55]. It is interesting that for a bursting neuron the minimal dynamical model is three-dimensional, and there are coupled slow–fast mechanisms [62], just as we have observed at currents close to the blue-sky catastrophe bifurcation, for the RCSJ model. Bursting dynamics has recently been studied in an all-to-all coupled network of single Josephson junctions, each within the RCSJ model [63]. The burst-like behavior observed here for the single junction may be an essential element of the emergent behavior seen in the globally coupled RCSJ model.

4. SPONTANEOUS AND CONTROLLED CHAOS SYNCHRONIZATION IN INTRINSIC JOSEPHSON JUNCTIONS

Synchronization properties of model systems containing large numbers of phase oscillators have many potential biophysical and other applications. Biophysical examples include networks of pacemaker cells in the heart and suprachiasmatic nucleus of the brain. In physical systems the phase dynamics of high-T_c superconducting materials continue to attract attention, since systems of intrinsic Josephson junctions form natural arrays of coupled phase oscillators. As such, they have the potential to act as systems in which various exotic synchronization effects may be naturally observed.

In our study [19] we have made a more detailed exploration of the parameter space containing regions of spontaneous chaos synchronization in the CCJJ + DC model of intrinsic Josephson junctions. Extensive regions of phase synchronization — corresponding to the Shapiro steps with zero charge density in the S-layers — are found through numerical simulation. By computing the Lyapunov exponent spectra, we have found that the spontaneous chaos synchronization occurs only within certain sub-regions that overlap with 'uncharged' steps in the I–V characteristics. The control is exerted through a phase shift, proportional total voltage, in the applied electromagnetic radiation. The effect of the control is found to be three-fold: (i) it tends to broaden the current interval over which lower harmonic Shapiro steps occur, (ii) it does not change the width in the current range over which the chaos synchronization occurs, and (iii) it makes the chaos synchronization more robust to noise. The chaos synchronization we reported here may be useful in any applications requiring more powerful, high-frequency, chaotic signals, such as in secure communication.

In Fig. 8 we show two views of a section in the $I-A$ parameter space. In Fig. 8, *a* the magnitude of the derivative of V, with respect to the dc-bias current I, is shown. This derivative is a convenient way of showing the Shapiro steps, on which it is zero (indicated by the black regions in the figure). Some of the main harmonics are shown by the white labels to the right bottom of the figure. In Fig. 8, *b* the chaos synchronization areas are shown for the corresponding region of the parameter space. Here one

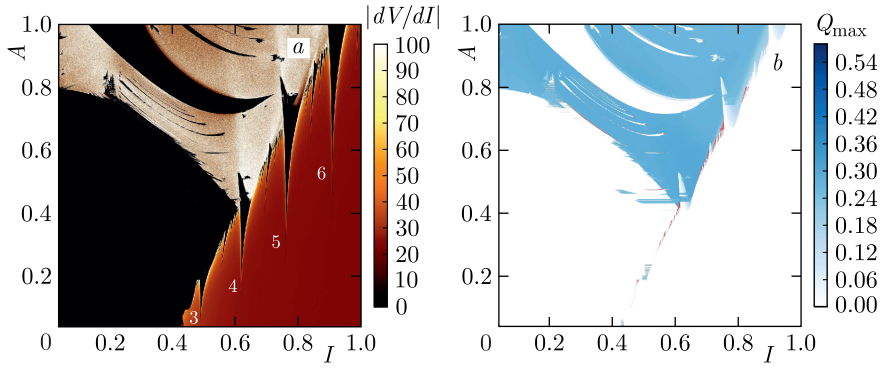

Fig. 8. *a*) Shapiro steps (or Arnold tongues), for $\beta = 0.3$. *b*) Corresponding regions of chaos synchronization (shown in red). Adapted from [19]

notices that the chaos synchronization occurs mostly at the edges of Shapiro steps, often where a main step gives way to an infinite sequence of higher harmonics (or subharmonics). Such infinite sequences of steps are well known in the literature on Josephson junctions and are loosely referred to as devil's staircases.

All of the chaos synchronization regions which we have observed in the present work [19] seem to be associated with such structured chaos. It appears that near the end of such "Svetlana" structures, where the steps start to span smaller and smaller current intervals, the in-between chaotic regions become fully synchronized, giving rise to the spontaneous chaos synchronization we observe. As one approaches the very end of the staircase (by increasing or decreasing the bias current), the regions of phase locking become insignificantly small and the structured chaos manifests itself as chaos synchronization.

5. CHAOS ALONG THE RC-BRANCH OF RLC-SHUNTED INTRINSIC JOSEPHSON JUNCTIONS

Recently, several different forms of chaos control have also been proposed, not only with the view of suppressing chaos but also to establish more robust synchronization between the junctions, which could be either in a chaotic state, for applications involving chaos synchronization, or in a regular state, where the junctions might be used, for example, to detect weak electromagnetic signals in the presence of noise, or to unscramble specific types of noise components within a noisy signal [28]. Synchronized Josephson junctions in high-temperature superconductors are promising candidates for sufficiently light and compact THz wave generators. While the radiation from a single Josephson junction is extremely weak, systems of synchronized Josephson junctions posses practically viable radiation power.

In [28] we have studied the appearance of chaos on the resonant branch of a shunted system of intrinsic Josephson junctions in a high-temperature

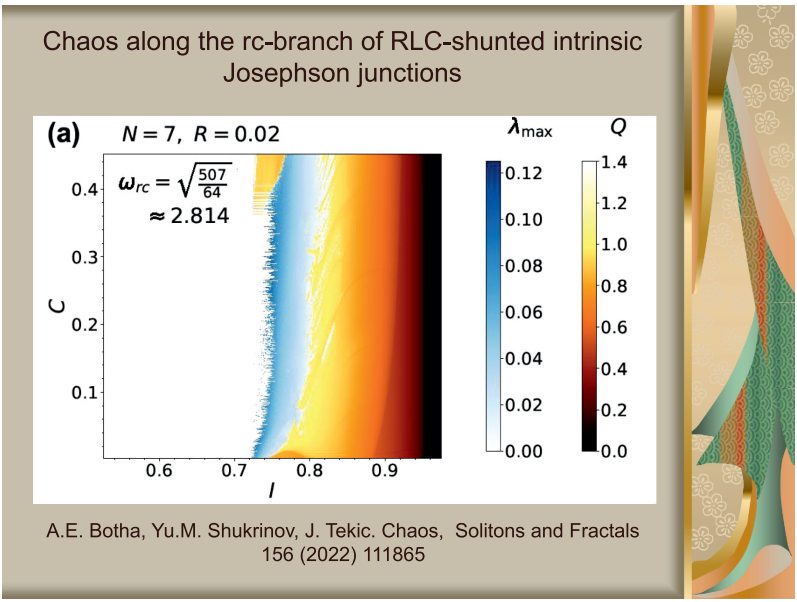

Fig. 9. Maximum Lyapunov exponent $\lambda_{\max}$ and maximum charge density Q along the resonant branch as a function of capacitance and decreasing DC bias current. Adapted from [28]

superconductor. Based on the calculated electrical characteristics of the superconducting layers and various indicators of chaos, such as Lyapunov exponents and Poincar? sections, the regions of current–voltage characteristics with a predominance of chaos, which are determined by the frequency of the resonant circuit, are indicated. The study of metric entropy and the maximum Kaplan–York dimension shows that the sizes of chaotic attractors associated with chaos do not reach a plateau, as in the case of systems with strong damping, but increase without limit with an increase in the number of Josephson junctions, demonstrating multidimensional chaos. The results obtained indicate the possibility of controlling chaos in studied systems. Color images of the maximum Lyapunov exponent and maximum charge density along the resonant branch as a function of capacitance and decreasing DC bias current are presented in Fig. 9.

6. STAIRCASE STRUCTURE AND CHAOS OF THE SFS φ_0 JOSEPHSON JUNCTIONS

We have discovered the specific ladder structures in the superconductor–ferromagnetic–superconductor (SFS) Josephson junction that appear under the action of a circularly polarized magnetic field [18]. In our study we consider two superconductors separated by a ferromagnetic layer, as shown

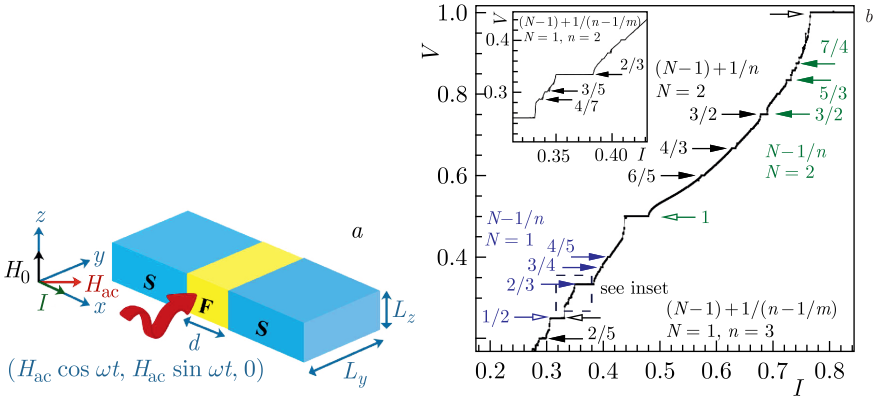

Fig. 10. *a*) Geometry of the SFS Josephson junction with cross-sectional area L_yL_z in uniform magnetic field H_0 and circularly polarized magnetic field H_{ac}. *b*) Subharmonic ladder structures in various parts of the current–voltage characteristic of the SFS junction at ferromagnetic resonance. Adapted from [18]

in Fig. 10. The coupling between the Josephson phase and magnetization in SFS junctions plays an important role in the dynamics of this system. In the presence of this coupling, the manifestation of ferromagnetic resonance in the dynamics of magnetization and critical current is shown in both nonlinear and linearized schemes. The width of the ferromagnetic resonance curve and the position of the resonant frequency are strongly affected by the ratio of the Josephson and magnetic energies.

Analytical formula was demonstrated for the appearance conditions of fractional steps in the I–V characteristic of the SFS Josephson junction. The DS structure is a universal phenomenon and appears in a wide variety of different systems, including infinite spin chains with long-range interactions, frustrated quasi-two-dimensional spin-dimer systems in magnetic fields, and even in the fractional quantum Hall effect. We consider that the subharmonic ladder structures can be used in various fields of superconducting spintronics, particularly, for detecting Majorana states in Josephson nanostructures. We note that in [45], authors reported the experimental observation of half-integer Shapiro steps in the strong ferromagnetic Josephson junction (Nb–NiFe–Nb) by investigating the current–phase relation under radio-frequency microwave excitation.

7. CHAOS AND BIFURCATIONS IN SUPERCONDUCTOR–FERROMAGNET–SUPERCONDUCTOR NANOSTRUCTURES

The possibility of achieving electric control over the magnetic properties of the magnet via Josephson current and its counterpart, i.e., achieving magnetic control over Josephson current, recently attracted much attention [20, 46–52].

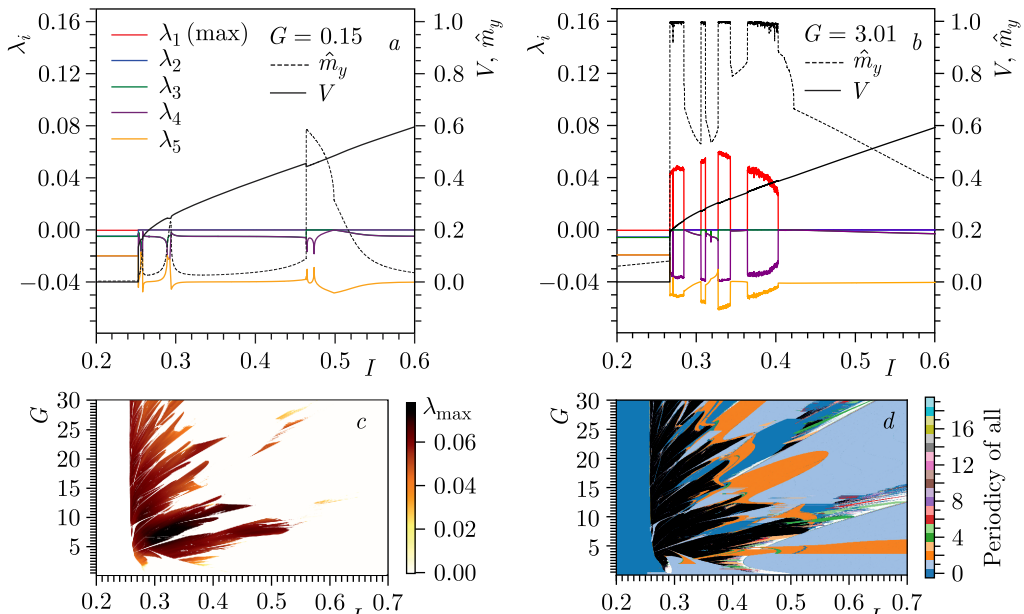

Fig. 11. *a*, *b*) The emergence of chaos in the φ_0 Josephson junction. Here V is the time-averaged voltage across the junction and $\widehat{m}_y$ is the maximum value of the y-component of the magnetization. λ_i are the Lyapunov exponents. *c*) The chaotic regions as functions of the ratio of Josephson energy to the magnetic energy, G. *d*) Demonstration of the periodicity and synchronization in the φ_0 Josephson junction. Here the regions marked by the blue color corresponding to zero indicate regions where not all of the state variables have the same periodicity, i.e., are not fully synchronized. Adapted from [31]

The ordinary (superconductor–insulator–superconductor) Josephson junction cannot exhibit chaos in the absence of an external ac-drive, whereas in the superconductor–ferromagnet–superconductor Josephson junction, known as the φ_0 junction, the magnetic layer effectively provides two extra degrees of freedom that can facilitate chaotic dynamics in the resulting four-dimensional autonomous system. The results of [31] show that, due to the conservation of magnetic moment magnitude, two of the numerically computed full spectrum Lyapunov characteristic exponents are always zero. The two-dimensional bifurcation diagrams, which are similar to traditional isospike diagrams, display the different periodicities and synchronization properties of the junction over parameter ranges that are experimentally accessible. It was demonstrated that as bias current I is reduced, the onset of chaos occurs shortly before the transition to the superconducting state.

In Figs. 11, *a* and *b* we illustrate the emergence of chaos in the φ_0 Josephson junction with increasing ratio G, of the Josephson energy to the magnetic energy. Here the full spectrum of Lyapunov exponents can be seen, with two being trivially zero for any I. In (*c*) we show the regions of chaos, as indicated by positive values of the maximal Lyapunov exponent, as funtions of G and the decreasing dc-bias I. Fig. 11, *d* demonstrates the periodicity and synchronization in the φ_0 Josephson junction.

8. HYSTERESIS AND CHAOS IN ANOMALOUS JOSEPHSON JUNCTIONS WITHOUT CAPACITANCE

Usually, overdamped Josephson junctions do not exhibit chaotic behaviour in their phase dynamics, either because the phase space dimension is less than three (as in the case of a single overdamped ac-driven junction) or due to the general tendency of systems to become less chaotic with increasing dissipation (as in the case of coupled overdamped junctions [16]). We have found that, in the case of strong spin-orbit coupling, the current–voltage characteristics of certain types of superconductor/ferromagnetic/superconductor φ_0 Josephson junctions are strongly influenced by the current-induced magnetization motion within the interlayers [30]. This influence may lead to chaotic regions and hysteresis, even though the junction is overdamped. We have also demonstrated that it is possible to induce switching between voltage states stemming from different magnetic modes via a current pulse. This switching behavior may open new perspectives for practical applications such as memory devices.

Figure 12 shows an example of the multistability that gives rise to this possibility of switching. In this case, the different branches seen in the CVCs, shown in (*a*), are due to the different magnetic modes, each having their own basins of attraction, as shown in (*b*) and (*c*).

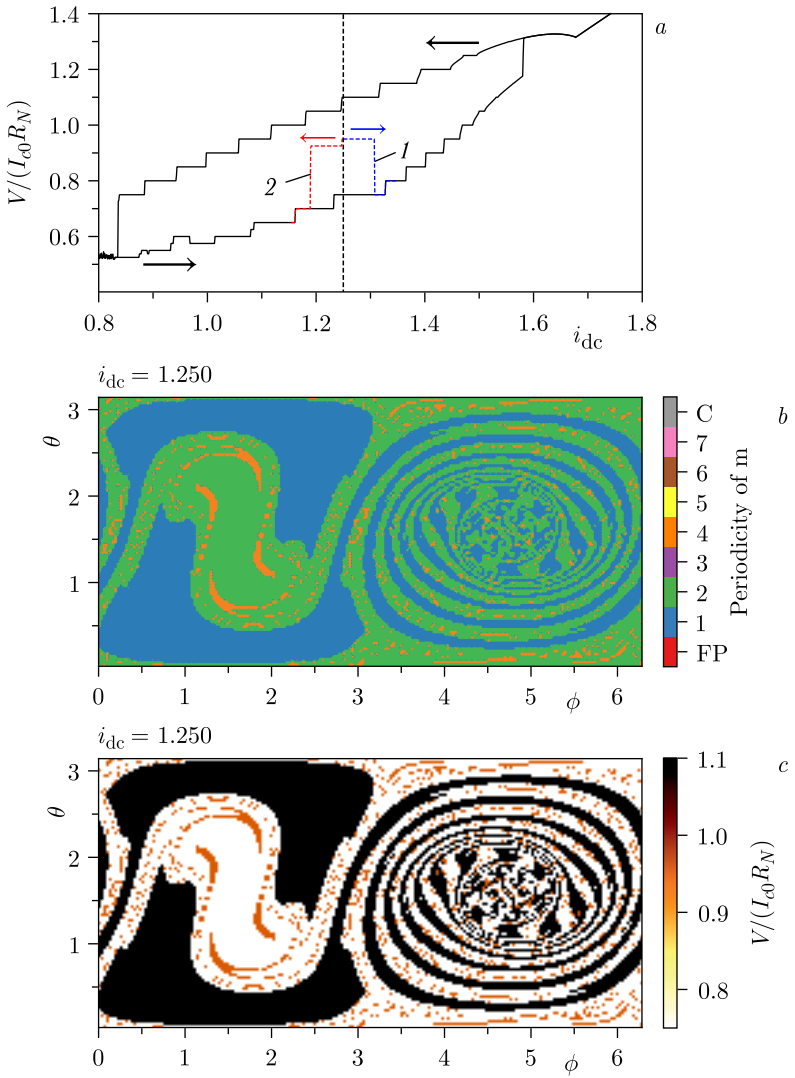

Fig. 12. *a*) Additional branches in the CVCs due to different magnetization modes. The arrows indicate the sweep directions of the dc-bias i_{dc}. The additional branches, shown by the dashed lines, were obtained by choosing a particular IC, at $i_{dc} = 1.25$, and then sweeping i_{dc} up (blue dashed line) and down (red dashed line). In both directions we find period 4 behavior in $\mathbf{m}(t)$. The vertical dashed grid line just shows the position of $i_{dc} = 1.25$. In (*b*) and (*c*), the basins of attraction corresponding to $i_{dc} = 1.25$ are shown for the periodicity of $\mathbf{m}(t)$ and the time averaged voltage, respectively. Adapted from [30]

9. BIFURCATION STRUCTURE AND CHAOS IN NANOMAGNET COUPLED TO JOSEPHSON JUNCTION

One of the most important tasks in the field of data coding and communication security is the development of methods for controlling and managing chaos. We have demonstrated a rich variety of periodic and chaotic behavior in the dynamics of the magnetic moment in the Josephson junction–nanomagnet (JJ–NM) system [29]. It was also shown that the chaotic behavior of the system can be controlled by applying an external periodic signal of the desired frequency and amplitude. It is assumed that such a system can be used as chaotic logic gates in computers based on chaotic systems. Irregular easy axis reorientation features are observed in numerical simulations of the nanomagnet coupled to the Josephson junction.

Figure 13, *a–c* (right) shows the bifurcation tree of the Poincaré section of the magnetization components ($m_{i-\mathrm{Poin}}$, $i = x, y, z$) as a function of G

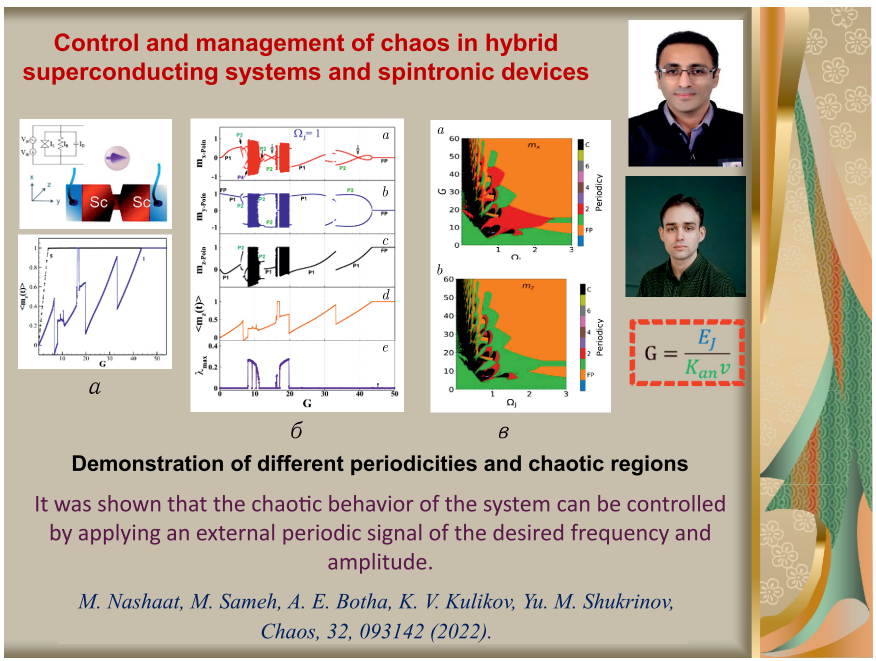

Fig. 13. Left column: a schematic diagram of the system (toP and the time-averaged magnetization as a function of G (bottom). Middle column: Bifurcation diagrams of the magnetization components (*a*) $m_{x-\mathrm{Poin}}$, (*b*) $m_{y-\mathrm{Poin}}$, (*c*) $m_{z-\mathrm{Poin}}$. The average value of the m_z–component is shown in (*d*), and (*e*) shows the largest Lyapunov exponent as a function of G at $\Omega_J = 1$. Right column: the two-dimentional bifurcation diagrams showing the periodicities in (*a*) m_x and (*b*) m_z. Portraits: Drs. M. Nashaat (top) and K. V. Kulikov (bottom). Adapted from [29]

before the complete reorientation. In our work we have described all types of motion which are revealed in the bifurcation tree. The transition from one type of motion to another, in this system, is accompanied by abrupt changes in the values of the average magnetization components. We demonstrate such changes in Fig. 13, *d* (right), where the irregular reorientation behavior of $< m_z(t) >$ appears before the complete reorientation. The $\lambda_{\max}$ calculation confirms the chaotic behavior of the magnetization (see Fig. 13, *e* (right). The intervals with positive values of $\lambda_{\max}$ coincide with the chaotic bands observed in the bifurcation diagrams.

The magnetic moment dynamics drastically changes at $\Omega_J > \Omega_F$ in comparison with the case $\Omega_J = \Omega_F$. Figure 13, *a–c* (right) shows the bifurcation trees of the magnetization as a function of G at $\Omega_J = 1.5$. Chaos does not appear and the bifurcation trees at $\Omega_J = 1.5$ demonstrate motions with different periods. The average $< m_z(t) >$ as a function of G in Fig. 13, *d* (right) reflects the transformation of the system from one kind of periodic motion to another.

10. CHIMERA STATES IN SYSTEMS OF JOSEPHSON JUNCTIONS

Following the relatively recent discovery of chimera states [53, 54], we were interested to know whether these exotic states may also exist is systems of Josephson junctions. In a mathematical sense, a chimera state refers to a certain type of behavior in any system that is composed of identical oscillatory elements. What makes it so unusual is that the chimera emerges as two or more distinct groupings, even though all the oscillators are identical. It is a form of emergent behavior in which, say, one group of oscillators may oscillate coherently (frequency synchronized) and the other, incoherently (not being synchronized).

In our studies of this phenomenon we were able to show that, over a considerable range of coupling strengths, a model of the intrinsic Josephson junctions with more extended coupling could support the occurrence of the so-called breathing chimeric states [4, 5]. Usually, the coupling within the CCJJ + DC model [55] only extends to the nearest neighbors. By extending the coupling within the CCJJ + DC model to include nonlocal (farther away) interaction between the junctions, we were able to demonstrate the existence of chimera states. The modified equations for the junctions with the extended coupling are

$$\frac{\mathrm{d}V_\ell}{\mathrm{d}}t = I + I_\ell^n - \sin\varphi_\ell - \beta\frac{\mathrm{d}\varphi_\ell}{\mathrm{d}t},$$

$$\frac{\mathrm{d}\varphi_\ell}{\mathrm{d}t} = V_\ell + 2\alpha\sum_{m=1}^{N} H_{\ell m}V_m, \qquad (2)$$

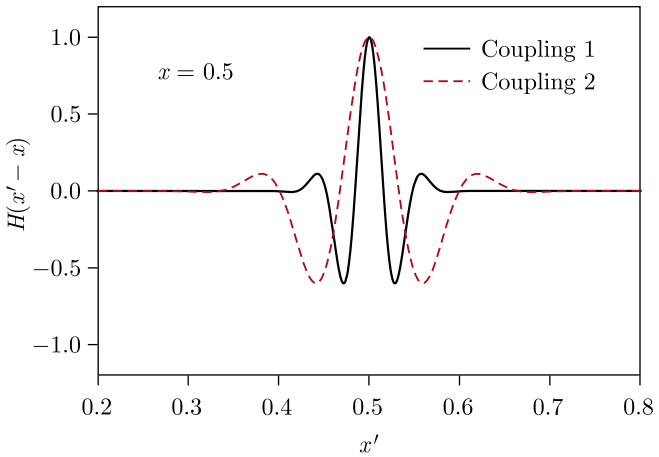

Fig. 14. Generalized coupling function at two coupling ranges. Junctions are positioned in a ring (periodic boundary conditions) withing the interval [0,1), where x_ℓ is the position of the ℓth junction. For mathematical convenience the coupling is treated as a continuous function, with the coupling matrix in Eq. (2) given by $H_{\ell m} \equiv H(x_\ell - x_m)$. The coupling in the original CCJJ + DC model [55] is reproduced exactly when the continuous coupling range is on the order of one junction separation, i.e., $\sim 1/N$

where N is the number of junctions and $H_{\ell m}$ is the generalized coupling, shown in Fig. 14.

In Figs. 15, *a* and *b*, the phase differences and velocities are shown for two different coupling types. These results correspond to a time domain with 10 000 dimensionless units after selecting the initial conditions. There are two clearly distinguishable areas in each drawing. In one region, the JJs are in a coherent rotating state, while in the other, they are in an incoherent rotating state. Our calculations show that the JJs in the incoherent region oscillate quasi-periodically with respect to the position of the coherent groups. Therefore, as the system evolves over time, the phase difference distributions, shown at the top of Fig. 15, *a* and *b*, move as a whole from $-\pi$ to π, like a rotating junction. While the relative phase difference of a coherently rotating JJ remains almost the same during rotation, the relative phase difference of an incoherent JJ oscillates almost periodically, i.e., quasi-periodically.

It is interesting to note that in the model system (2) the nonlocal coupling is between the voltage differences V_ℓ of the different junctions. This is in contrast to the usual type of coupling that leads to chimera states in, for example, the Kuramoto–Sakaguchi model of phase oscillators, in which the nonlocal coupling is directly between the phases, φ. Thus, in the present model there is a *second-order* nonlocal coupling, since $V_\ell = \dot{\varphi}_\ell$ for the uncoupled junctions (Eq. (2) with $\alpha = 0$).

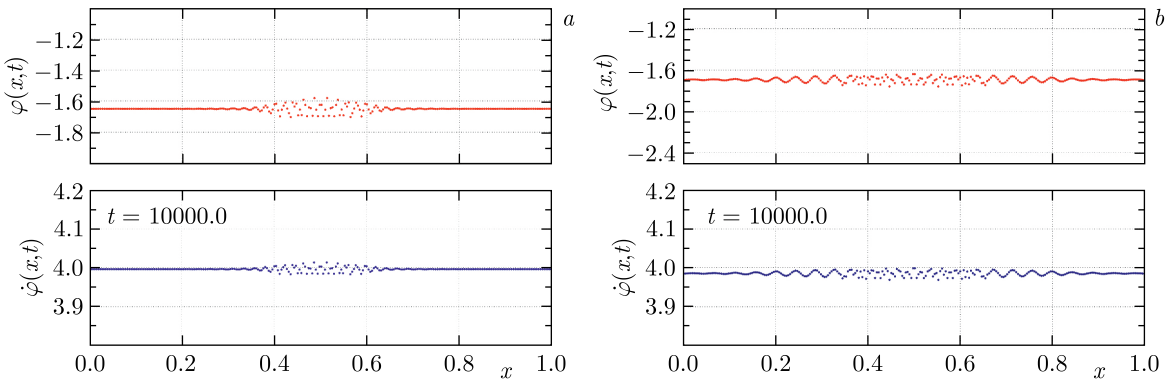

Fig. 15. Quasi-periodic pulsating chimera states corresponding to (*a*) Coupling 1 and (*b*) Coupling 2, seen in Fig. 14. In both figures, the bias current was $I = 0.8$, with $\alpha = 0.3$ and $\beta = 0.2$ and $N = 256$. The top figures show the instantaneous phase differences for each junction at $t = 10\,000$. The bottom figures show the time averaged velocities of the junctions, averaged over $\Delta t = 1000$. Junctions between about 0.35 and 0.65 are characterized by incoherence among their phases, while those in the remaining region rotate coherently. Adapted from [5]

11. RESONANCE PHENOMENA AND CHARGING OF SUPERCONDUCTING LAYERS IN HIGH T_C SUPERCONDUCTORS

One of the most interesting and promising studies of modern science is research in the field of high-temperature superconductivity. High-temperature superconductors have a layered structure consisting of thin superconducting (S) layers separated by the dielectric ones. Because the thickness of superconducting layers is comparable with a Debye screening length, the electric charge cannot be screen there. The issue of the appearance of the electric charge in the superconducting layers is of fundamental importance and it is not completely clarified till now. The presence of charge and the nature of its relaxation determine nonequilibrium phenomena in these systems.

In our collaborative paper [14], we have found that the coupled system of Josephson junctions under external electromagnetic radiation demonstrates a cascade of parametric instabilities. These instabilities, in particular, appear along the I–V characteristics within bias current intervals corresponding to the Shapiro step subharmonics and lead to charging of the superconducting layers. The amplitude of the charge oscillations increases with increasing external radiation power. We demonstrate the existence of longitudinal plasma waves at the corresponding bias current values. An essential specific feature of the parametric instabilities in the case of subharmonics is the lower amplitude of radiation that is needed for the creation the longitudinal plasma wave. This fact gives a unique possibility to create and control of the longitudinal plasma waves in layered superconductors. We propose a novel experiment for studying parametric instabilities and the charging of superconducting layers based on the simultaneous variation of the bias current and radiation amplitude.

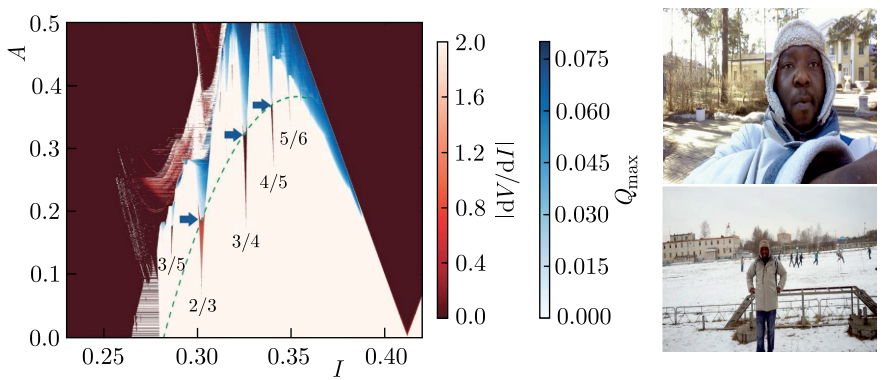

Fig. 16. "Charging" of the Shapiro step subharmonics as a function of radiation amplitude and dc bias current. Arrows indicate the points when the steps are becoming "charged". The green dashed line stresses the parabolic dependence of $A(I)$ along the transition boundary. Pictured on the right is a co-author Dr. Hermann Azemtsa Donfack on a research visit to Dubna. Adapted from [14]

To visualize the subharmonic steps clearly, and over a continuous range of the relevant parameter values, we have plotted, using the red color map in Fig. 16, the magnitude of the differential resistance as a function of the radiation amplitude and bias current.

To see when charge develops on each of the step we have superimposed a plot of the magnitude of the maximum charge in the S–layers $Q_{\max}$ on the same figure, using the blue colormap. Regions of no charge, or charge in excess of 0.08 (as may occur for inner branches), have been rendered as being transparent, so as not to obscure the underlying plot. The V-shape that can be seen on the right hand side of the figure is the main SS harmonic, which has a linearly increasing width for small A.

Important results were found in [11], demonstrating that the chaotic features are triggered by the coupling between different junctions in the stack. While the radiation is well known to produce chaotic effects in the

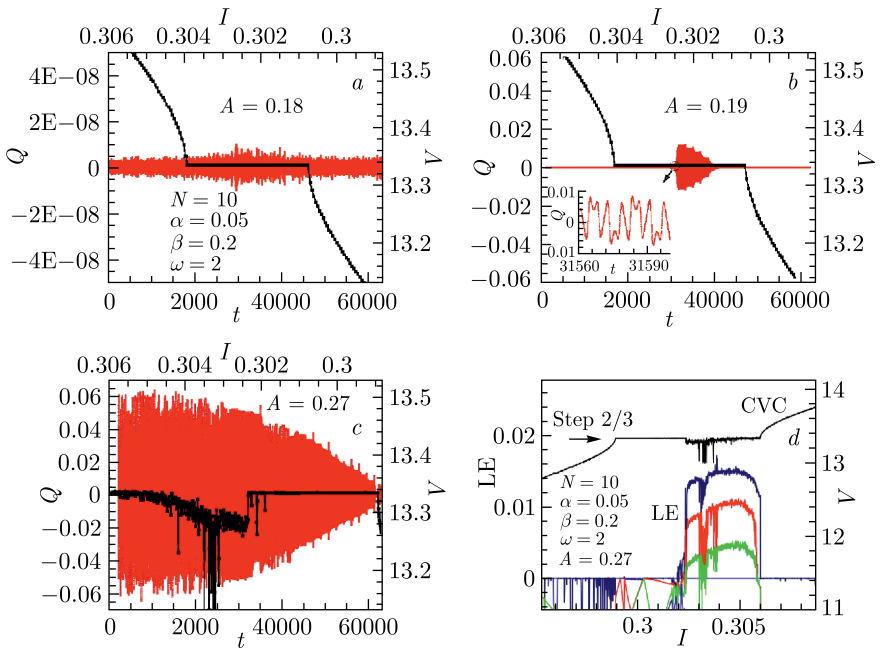

Fig. 17. Charge–time dependence (left and lower axes) together with I–V characteristics (black curves, right and upper axes) with increasing amplitude of radiation: *a*) $A = 0.18$; *b*) $A = 0.19$; *c*) $A = 0.27$. *c*) Manifestation of the chaotic features in the I–V characteristic. *d*) Lyapunov exponents (LE, left and lower axes) and I–V characteristic (CVC, right and lower axes) of the stack with 10 JJs at $\omega = 2$ and $A = 0.27$ around of the Shapiro step subharmonic 2/3. The regions in bias current for which the LE become positive correspond to regions over which the phase-locked step in the underlying I–V characteristic have been replaced by chaotic dynamics. Adapted from [11]

single junction, the effect of inter-junction coupling is fundamentally different and it can lead to the onset of chaos via a different route to that of the single junction. We have demonstrated the creation of a longitudinal plasma wave along the stack of junctions and proved that the observed chaos is induced by the coupling between the junctions. The important new point is that the use of Shapiro step subharmonics may allow the longitudinal plasma waves to be excited at low radiation power. The appearance of charge in the superconducting layers in the current interval corresponding to the SS harmonics was shown in [56].

In Fig. 17, we demonstrate the appearance and growth of charge in the first superconducting layer of the stack, within a current interval corresponding to the subharmonic step 2/3, with an increase in the amplitude of radiation. With increase in A the value of charge grows and it eventually occupies the total current interval corresponding to the SSS. We see this in Fig. 17, *c*, which shows the result for $A = 0.27$. At this largest A we see fragmentation of the SS subharmonic. To confirm the chaotic behavior of the stack of Josephson junctions at $A = 0.27$, we demonstrate the Lyapunov exponent spectrum of the system in Fig. 17, *d* which shows all nontrivial LEs together with I–V characteristic as functions of the dc-bias current for the stack with ten JJs at $\omega = 2$ and $A = 0.27$ around the subharmonic step. We see that one portion of the step 2/3 in I–V characteristics is associated with hyperchaotic dynamics in the coupled junctions. Three LEs (blue, red and green online) are positive within a subinterval of the current interval corresponded to this SS subharmonic.

12. CHARGING OF SUPERCONDUCTING LAYERS IN SHUNTED HIGH T_C SUPERCONDUCTORS

Results of our study of the resonance phenomena in high-temperature superconductors allowed us to propose a novel method for the determination of charging the superconducting layers based on the voltage dynamics [17]. The phase dynamics and I–V characteristics were investigated in detail when the Josephson frequency approaches the frequency of the resonance circuit. We have demonstrated a realization of parametric resonance through the excitation of a longitudinal plasma wave, within the bias current interval corresponding to the resonance circuit branch. Manifestation of S-layer charging by changing the amplitude of voltage oscillations is presented in Fig. 18, where part of I–V characteristics and maximal voltage amplitude without added noise (*a*) and with added noise (*b*) are demonstrated. It is found that the temporal dependence of the total voltage of the stack, and the voltage measured across the shunt capacitor, reflect the charging of superconducting layers. The amplitude of the voltage oscillations, measured at each value of the base current, changes the slope depending on the bias current when a charge occurs. This phenomenon might be useful as a means of detecting such charging experimentally.

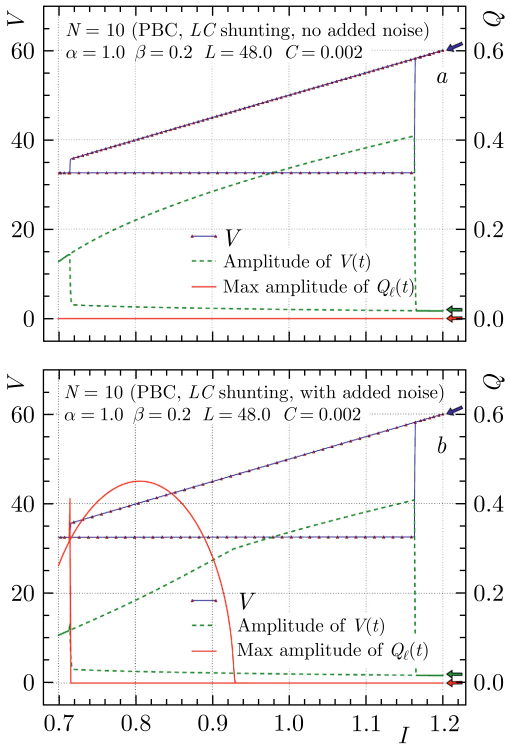

Fig. 18. Manifestation of S-layer charging by changing amplitude of voltage oscillations. *a*) Part of I–V characteristic and maximal voltage amplitude without added noise. *b*) The same as in (*a*) with added noise. In both figures one current cycle is performed: $1.2 \longrightarrow 0.7 \longrightarrow 1.2$. The starting value ($I = 1.2$) and initial direction of the current cycle (decreasing current) is indicated by the arrows, to the right of the figure. Adapted from [17]

Figure 19 shows the time dependence of the charge in the region of the resonant branch [17]. As can be seen in Fig. 19, *a*, at $L = 42$ there is no electric charge on the superconducting layer. The amplitude of the charge on the capacitor monotonically increases with increasing current until the resonance point $\omega_J = \omega_{rc}$. A charge appears on the superconducting layers and increases with increasing L. At $L = 45$ ($\omega_{rc} = 3.367$), as we see in Fig. 19, *b*, the charge on the superconducting layer exists simultaneously with the charge on the capacitor. Note that the interval of monotonic increase in the charge amplitude is highlighted by a dotted line. We see an area of reduced amplitude in the time dependence of the capacitor charge. The region with reduced amplitude is clearly shown in Fig. 19, *c* at $L = 48$. The analysis of the charge distribution along the stack shows that a longitudinal plasma wave appears with a wavelength of $\lambda = 2d$, where d is the stack period. The dotted

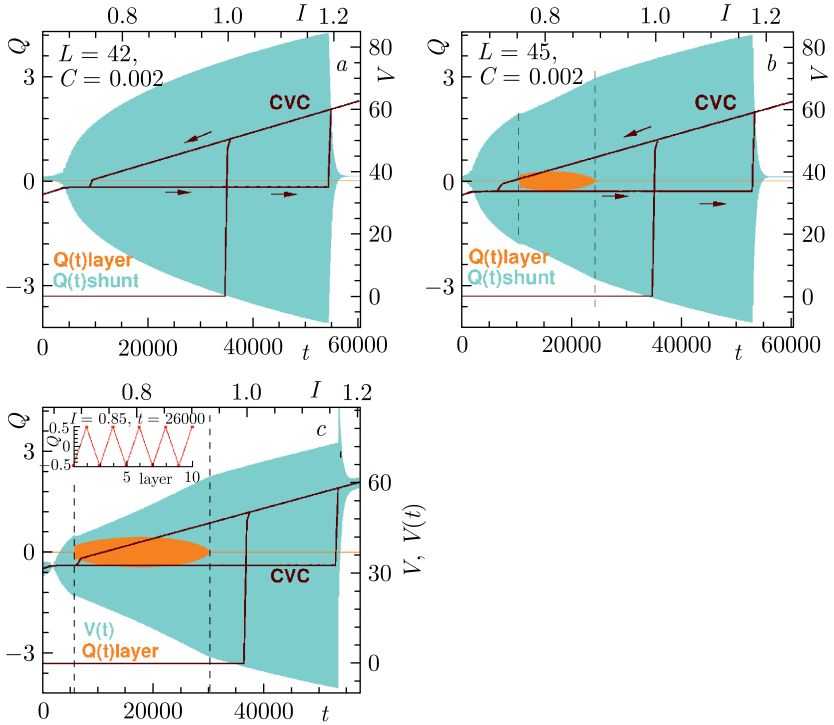

Fig. 19. Time dependence of the charge on the shunt capacitor (light, blue) and the charge on the superconducting layer (dark, orange) together with the corresponding part of the current–voltage characteristic including the resonant branch, calculated for a 10 JJs shunted system $C = 0.002$, *a*) $L = 42$, *b*) $L = 45$. *c*) Time dependence of voltage and charge with the corresponding part of the current–voltage characteristic for a system of ten JJs shunted by a resonant circuit with a frequency of $\omega_{rc} = 3.2596$. The inset shows a longitudinal plasma wave with a wavelength of $\lambda = 2$, which is formed in the stack at $I = 0.85$. Adapted from [17]

line shows the current interval in which a longitudinal plasma wave exists in the stack. A decrease in ω_{rc} leads to an increase in this current interval.

Shunting of Josephson structures leads to the appearance of additional resonances and opens up new possibilities in controlling their properties. In our joint study [27] the double and triple resonances were demonstrated and their influence on the appearance of an electric charge in superconducting layers was shown. For a larger number of junctions, shunting causes the appearance of a charge in the states corresponding to the upper and resonant branches of the current–voltage characteristic. A transformation of a traveling wave into a standing longitudinal plasma wave was observed in the system.

As it was demonstrated, LC shunting leads to the formation of a resonant branch on the current–voltage characteristic [13, 17]. The calculated

current–voltage characteristic is presented in Fig. 20 and it was obtained by changing the current along $01OEBABCDEBF0$. The current–voltage characteristic demonstrates the resonant branch of AC as a result of the resonance of Josephson oscillations and natural oscillations of the formed oscillatory circuit. The resulting resonant branch is the stable side of the resonant peak, since the other side has a negative slope and is therefore unstable. This peak corresponds to parallel resonance. In the case of series resonance, the resonance peak is generated in the opposite direction. The dotted line in Fig. 20, *a* corresponds to the unstable part of the resonant peak and the top of the peak is indicated by the letter C.

The selected shunt parameters $L = 0.2$ and $C = 1.25$ lead to the natural frequency of the resonant circuit $\omega_{rc} = 3$. At $V = 3$, the reactance of the circuit is $Z(\omega)^{-1} = (1/j\omega C_j)^{-1} + (j\omega L + 1/j\omega C)^{-1}$ tends to infinity. At this point we see a voltage jump on the current–voltage characteristic.

In particular, the influence of external radiation on the dynamics of a Josephson junction shunted by an LC circuit was studied. It was shown that the dependence of the width of the Shapiro step on the amplitude of external radiation changes dramatically when the step is located on the resonant branch. We believe that the results obtained can be useful for methods and technologies that use the response of Josephson junctions to microwave radiation, in particular, in quantum metrology for volt standards.

The dependence of the Shapiro step width on the amplitude of external radiation A_R at its frequency $\omega_R = 3$ is presented in Fig. 20, *b*, where the dots indicate the result of the numerical calculation and the squares correspond to the theoretical formula. Note that the amplitude dependence of the width of the Shapiro step for a JJ with shunting is designated SS-rc and without a shunt SS. An important result is that when the frequency of external radiation is equal to the frequency of the resonant circuit, then the maximum width of the Shapiro step can be obtained at significantly lower amplitudes compared to the case without shunting.

Plasma waves are the interesting objects which appear in Josephson nanostructures. We have investigated the temporal dependence of the charge oscillations at different values of bias current, as the bias current is swept up and down along I–V characteristic. Figure 20, *c* shows the part of I–V characteristic including rc-branch for a stack with $N = 30$, together with maximal amplitude of charge in the S-layers. The symbols indicate the points where the charge–time dependence was recorded. Results of our analysis of some of these points are presented in Fig. 20. With sweeping down along the outermost branch, we observe a travelling wave along the stack. Initially the travelling wave has a wavelength $\lambda = 30$ at $I = 0.97$, but transforms to another travelling wave with $\lambda = 15$ at $I = 0.96$. After the bifurcation to the rc-branch, we observe a standing wave with wavelength $\lambda = 2$ at $I = 0.71$. This wave exists along the rc-branch in the current interval corresponding to the charge dome. Outside of the rc-branch we only observe charge oscillations at the noise level.

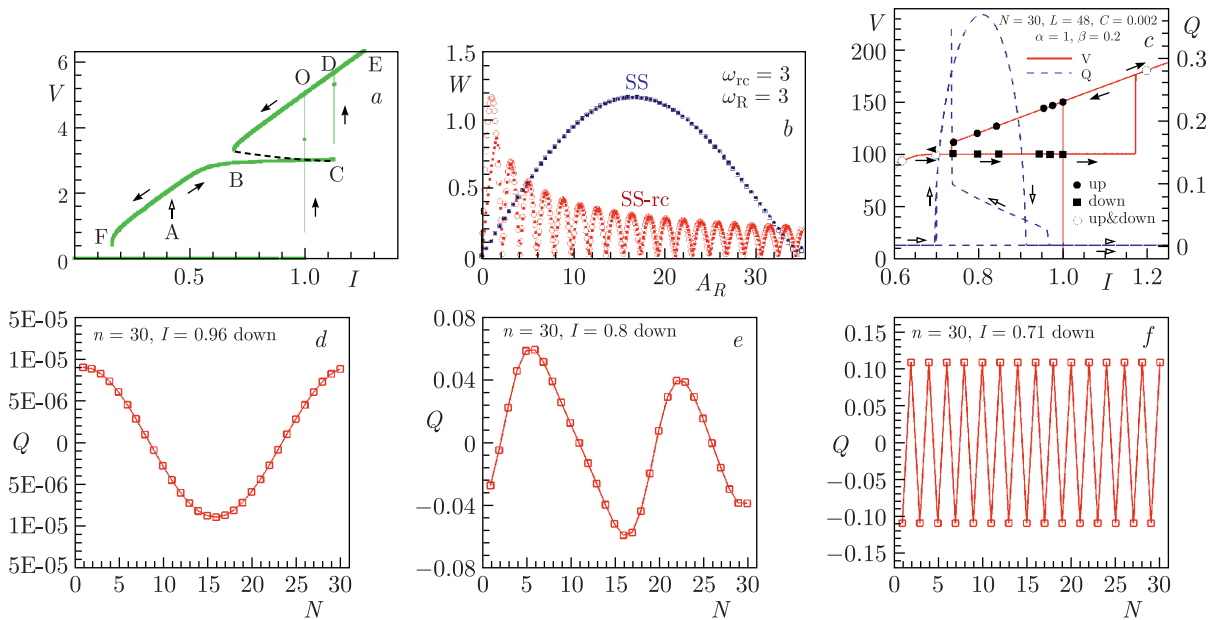

Fig. 20. *a*) Current–voltage characteristics of a shunted JJ with an increase and decrease in the bias current. The arrows indicate the direction of current change. Here there is a resonant circuit (rc) branch between points A and C. The dotted line corresponds to the unstable part of the resonant peak. *b*) Amplitude dependence of the width of the Shapiro step, for $\omega_R = 3$. *c*) The part of CVC including rc-branch for a stack with $N = 30$, together with maximal amplitude of charge oscillations in the S-layers. The symbols indicate the points at which the charge-time dependence has been tested. *d–f*) Realizations of LPWs in the stack with $N = 30$, for a downward sweeping current corresponding to the CVC presented in (*a*). Adapted from [27]

13. SPINTRONIC EFFECTS IN ANOMALOUS JOSEPHSON JUNCTIONS

An important challenge in superconducting spintronics dealing with the Josephson junctions coupled to magnetic systems is the achievement of electric control over the magnetic properties by the Josephson current and its counterpart, i.e., the achievement of magnetic control over the Josephson current [46, 51, 57]. An example is a full magnetization reversal in a superconductor/ferromagnet/superconductor (SFS) structure with spin-orbit coupling by adding an electric current pulse [48]. Such a reversal may be important for certain applications in quantum computing. We have demonstrated in this field interesting and important results by concentrating our work on superconducting structures with magnetic materials. An important place of joint studies was occupied by topological and chaotic phenomena in different types of Josephson structures.

In [24] the switching of magnetization by electric current pulse in the φ_0 Josephson junction formed by ordinary superconductors and a magnetic noncentrosymmetric interlayer is studied. Based on the Landau–Lifshits–Gilbert and resistively shunted junction model equations we build an analytical description of the magnetization dynamics induced by an arbitrary current

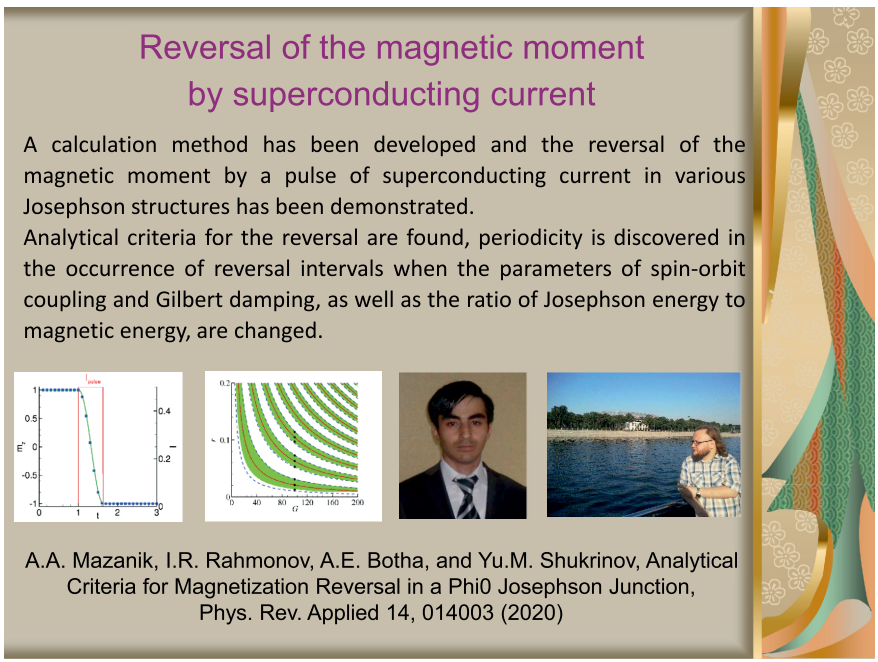

Fig. 21. A slide from a presentation related to [24]. The photographs at the bottom show the co-authors I. R. Rahmonov (left) and A. A. Mazanik (right)

pulse, as shown at the left bottom of Fig. 21. We formulate the criteria for magnetization reversal and, using the obtained results, the form and duration of the current pulse are optimized. The analytical and numerical results are in excellent agreement at $GrIp \gg 1$, where G is a Josephson-to-magnetic energy ratio, r is a strength of spin-orbit interaction, and I_{pulse} is a value of the current pulse. The analytical result allows one to predict magnetization reversal at the chosen system parameters and explains the features of magnetization reversal in the $G{-}r$ and $G{-}\alpha$ diagrams, where α is the Gilbert damping. We propose to use such a φ_0 Josephson junction as a memory element, with the information encoded in the magnetization direction of the ferromagnetic layer.

In the [21] we have demonstrated three types of effects leading to magnetization reversal in a ferromagnetic layer, including changes in the magnetic moment by a superconducting current pulse (see Fig. 22, *a*),

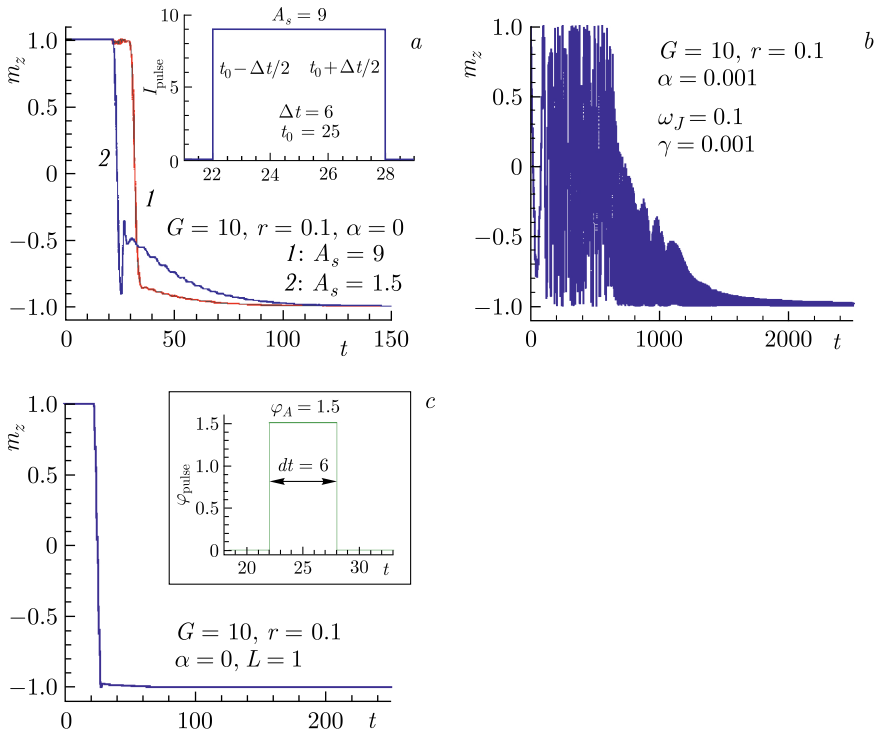

Fig. 22. *a*) Dynamics of the m_z magnetization component for a system with a rectangular current pulse for two pulse amplitudes. The inset shows the pulse shape. *b*) Magnetization reversal by linearly decreasing the bias voltage for $\omega_J = 0.1$, $\gamma = 0.001$ and model parameters $G = 10$, $r = 0.1$, $\alpha = 0.01$. *c*) Magnetization reversal in an RF SQUID by an external magnetic field pulse shown in the inset. Adapted from [21]

a linearly decreasing bias voltage in the φ_0 junction (see Fig. 22, *b*), and an external magnetic field pulse in an rf SQUID with φ_0-junction (see Fig. 22, *c*). The observed features can find application in various areas of superconducting spintronics.

14. RE-ORIENTATION OF THE EASY AXIS IN A φ_0 JUNCTION

Another interesting result in the framework of our collaboration was obtained by studying manifestation of Kapitza pendulum features in SFS junctions. As it is known, Kapitza's pioneering work [58] initiated the field of vibrational mechanics, and his method was used to describe periodic processes in a variety of different physical systems, like atomic physics [59–62], plasma physics, optics [63], condensed matter physics, biophysics [64] and cybernetical physics (see [65–70]). In nonlinear control theory the Kapitza pendulum is used as an example of a parametric oscillator that demonstrates the concept of "dynamic stabilization".

In [20] we study theoretically a dynamics of the φ_0 Josephson junction with direct coupling between magnetic moment and Josephson current, which

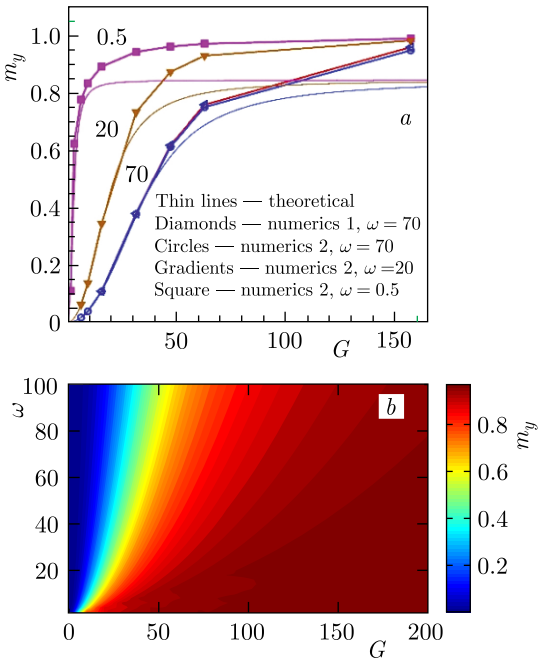

Fig. 23. *a*) Re-orientation of the easy axis of a ferromagnet. Comparison of theoretical and numerical calculation data for certain values of the Josephson frequency and the ratio of Josephson and magnetic energies (G). *b*) The $\omega - G$-diagram for averaged m_y shown by color. Adapted from [20]

shows features reminiscent of a Kapitza pendulum. We find that, starting with the magnetization along the z-axis, the character of the magnetization dynamics changes crucially as a stable position of the magnetic moment is realized between the z- and y-axes, depending on the values of the system parameters. Changes in critical current and spin-orbit interaction lead to different stability regions for the magnetization. Excellent agreement is obtained between analytical and numerical results at low values of the Josephson to magnetic energy ratio.

As is well known, the most important characteristic of the Josephson structure measured experimentally is its current–voltage characteristic. For the first time, subharmonic ladder structures were found in the current–voltage characteristics, which are due to the influence of the magnetization dynamics on the phase difference in the Josephson junction [18, 20]. Such structures can be used in various fields of superconducting spintronics. They are sensitive to changes in the periodicity in the dynamics of the system and can serve as an indicator of various exotic states. In particular, they can be used to detect Majorana bound states in Josephson nanostructures.

Over the past few years, we have studied various Josephson nanostructures and obtained a number of original results [20]. The manifestations of the Kapitza pendulum properties were observed, in particular, the reorientation of the easy axis of the ferromagnet with changes in the critical current and spin-orbit interaction. Good agreement between analytical and numerical results was obtained for certain values of the Josephson frequency and the ratio of Josephson and magnetic energies.

Variation of average m_y as a function of frequency ω and G is shown in Fig. 23, *a*. We see that an increase in G makes orientation of m_y along y-axis stable, but that the frequency dependence shown in Fig. 23, *b* differs from the characteristic Kapitza pendulum behavior.

15. KINK STRUCTURE IN THE I–V CHARACTERISTICS OF A φ_0 JUNCTION

The φ_0 junction demonstrates a rich variety of dynamical states determined by parameters of the Josephson junction and the intermediate ferromagnetic layer. In [25] we found several peculiarities in the maximal amplitude of magnetic moment $\widehat{m_y}$, taken at each value of the bias current, which we correlate to the features of the I–V characteristics of the φ_0 junction. In Fig. 24 we show a part of I–V characteristics together with the maximal amplitude $\widehat{m_y}$ with decrease in bias current at $I > I_c$. An interesting feature of this $\widehat{m_y}(I)$-dependence are the kinks shown by the arrows.

We show that a kink behavior in the bias current (voltage) dependence of $\widehat{m_y}$ along the I–V characteristics is related to the changes in the dynamical behaviour of the magnetization precession in the ferromagnetic layer. We also demonstrate a transformation of the magnetization specific trajectories along the I–V curve, magnetization composite structures, and hysteretic behavior in the bias current dependence of $\widehat{m_y}$.

Different types of magnetization trajectories in the $m_y - m_x$, $m_z - m_x$, and $m_z - m_y$ planes, realized along the I–V characteristics were found in [71], such as "apple", "sickle", "mushroom", "fish", and "moon", called like that for distinctness. But the kinks in $\widehat{m_y}$ and their origin were not discussed at that time. It was mentioned there that the specific trajectories demonstrate a unique possibility of controlling the magnetization dynamics via external bias current. Here we demonstrate the similarity in the appearance of the different kinks and stress that their origin is related to the transformation in the magnetization dynamics. In Fig. 24 we show the magnetization trajectories around the kink in the R_2 region, which present the "apple" type at $I = 0.6$ before the kink and the "mushroom" type after kink at $I = 0.555$. The FFT analysis shows the doubling of the period of trajectories in case of the "mushroom".

Results in the regular region R_1, at $I = 0.95$ (a, b) and $I = 0.75$ (c, d), i.e., to the right and left sides of the kink, respectively, are shown in Fig. 24. We find that the kink is the bifurcation point between the two types of trajectories, i.e., as the system goes from period one to period two behavior. At $I = 0.75$ an additional frequency $f = f_J/2$ appears in comparison to the case at $I = 0.95$, confirming the period doubling.

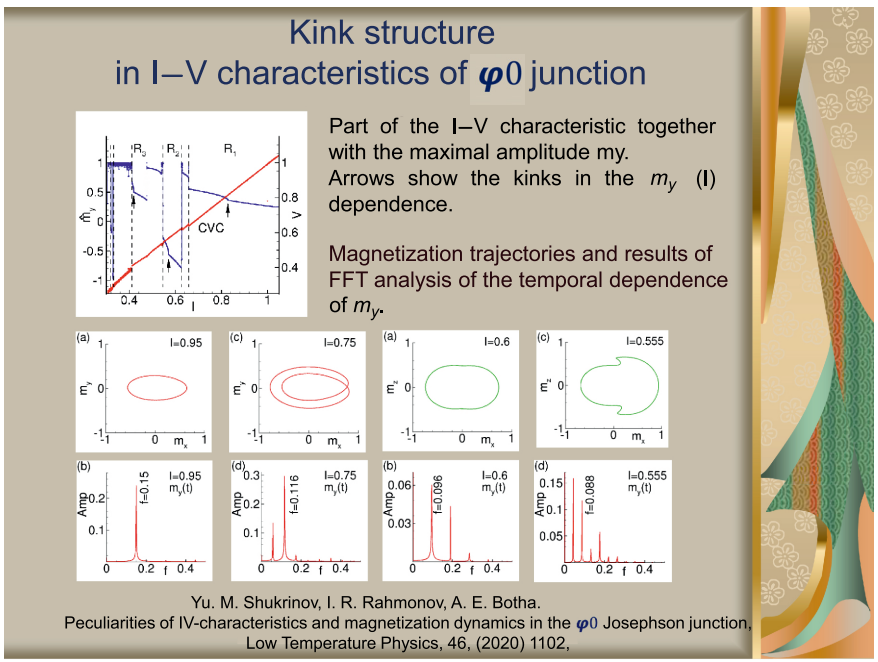

Fig. 24. Demonstration of the kink structure in the current–voltage characteristics of a φ_0 junction. Adapted from [25]

Due to the correlations between features of $\widehat{m_y}$ and the I–V characteristics, the presented results open a way for the experimental testing of the peculiar magnetization dynamics which characterize the φ_0 junction.

16. THE OVERDAMPED $DC + AC$ DRIVEN FRENKEL–KONTOROVA (F–K) MODEL

The $ac + dc$ driven F–K model is well known as a model of the sliding charge-density wave systems in the radio frequency field and Josephson junction systems in the microwave field. A detailed comparative analysis between the chaotic behavior of the F–K model and the JJs systems is helpful in reproducing the chaotic phenomena observed in the real systems and in identifying the common mathematical features that lead to the chaotic behavior in both models.

One common feature is the so-called devil's staircase, which has been observed in the I–V characteristics of the Josephson junction and in the average velocity $\overline{v}$ as a function of average driving force $\overline{F}$ in the underdamped

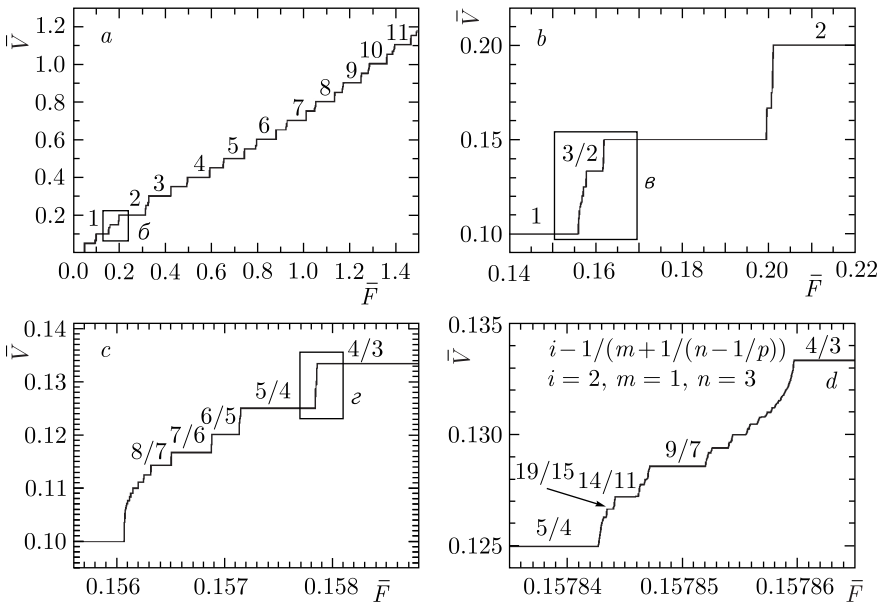

Fig. 25. *a*) The average velocity as a function of the average driving force $\overline{v}(\overline{F})$ for $N = 8$, $K = 4$, $\nu_0 = 0.2$, $\omega = \frac{1}{2}$, $r = 0.5$, and $F_{ac} = 1.1$. Here N is the number of particles, K is the pinning strength, ν_0 is the frequency of the ac drive, ω is the winding number, and $(-1 < r < 1)$ is deformation parameter for the substrate potential ($r = 0$, corresponding to a sinusoidal substrate potential). Numbers mark harmonic and subharmonic steps. High resolution views (*b*), (*c*) and (*d*) represent devil's staircase of the selected area. Adapted from [16]

F–K model. In Fig. 25, the staircase structure of the response function $\overline{v}(\overline{F})$ is presented at a fixed, relatively large, amplitude ($F_{ac} = 1.1$) of the ac force, while the dc force is slowly varied (note, $\overline{F} = F_{dc}$). The magnification of the steps between the first and the second harmonics in Fig. 25, *a*, shows that an infinite series of subharmonic steps (the devil's staircase) start to appear in *b*, *c* and *d*.

In our work we have shown that the devil's staircase structure may arise from the complete mode locking of an entirely nonchaotic system, i.e., the overdamped dc + ac driven Frenkel–Kontorova model with a deformable substrate potential [16]. Even though we found no chaos in this model, a hierarchical ordering of the Shapiro steps was made possible through our use of a previously introduced continued fraction formula. The absence of chaos, deduced here from Lyapunov exponent analyses, was attributed to the overdamped character and the Middleton no-passing rule. A comparative analysis of a one-dimensional stack of Josephson junctions confirmed the disappearance of chaos with increasing dissipation. Other common dynamic features were also identified through this comparison. A detailed analysis of the amplitude dependence of the Shapiro steps revealed that only for the case of a purely sinusoidal substrate potential did the relative sizes of the steps follow a Farey sequence. For nonsinusoidal (deformed) potentials, the symmetry of the Stern–Brocot tree, depicting all members of particular Farey sequence, was seen to be increasingly broken, with certain steps being more prominent and their relative sizes not following the Farey rule [16].

17. SUBHARMONIC STEPS, CHAOS, AND HYSTERESIS IN THE F–K MODEL

We have also examined the effects of the inertial terms on the dynamics of the dc + ac driven Frenkel–Kontorova model [22]. As the mass of particles was varied, the response of the system to the driving forces and appearance of the Shapiro steps were analyzed in detail. Unlike in the overdamped case, the increase in mass led to the appearance of the whole series of subharmonic steps in the staircase of the average velocity as a function of average driving force in any commensurate structure. At certain values of parameters, the subharmonic steps became separated by chaotic windows while the whole structure retained scaling similar to the original staircase. The mass of the particles also determined their sensitivity to the forces governing their dynamics. Depending on their mass, they were found to exhibit three types of dynamics, from dynamical mode-locking with chaotic windows, through to a typical dc response, to essentially a free-particle response. Our analysis of these dynamics in both the upforce and downforce directions showed that the system may not only exhibit hysteresis, but also that large Shapiro steps may appear in the downforce direction, even in cases for which no dynamical mode-locking occurred in the upforce direction [22].

18. SYNCHRONICITY IN ELECTRICAL POWER GRIDS

One of the key requirements to avoid cascading failures, i.e., blackouts, in power transmission grids, is their ability to operate stably in a synchronous mode [72–74]. In recent times, however, growing demands made on existing power grids, such as increasing loads and pressure to incorporate more environmentally-friendly energy sources, like wind and solar [75], have threatened to collapse entire grids. In South Africa, for example, in order to avoid a complete collapse, very high levels of the so-called "load shedding" have had to be implemented, at a huge cost to the economy [76]. In this context, the study of electrical power grids, with the view of developing better future grids (as discussed in [77], for example), is a national, if not international, priority.

In December of 2019, we were awarded three years of mobility funding towards a new project involving the studiy of synchronization phenomena in networks of coupled Josephson junctions. The main motivation for this project was the idea that coupled systems of Josephson junctions could potentially be used to create a model of real power grids, each Josephson junction playing the role of one element in the real grid, i.e., either a power generator or consumer. Unfortunately, to the the occurrence of the Covid-19 pandemic at the start of 2020, this project was considerably delayed, since the funding was specifically for collaborative visits, and for a long time all travel between South Africa and Russia was prohibited. Nevertheless, after the pandemic work did commence and we managed to publish a short proceeding on the effects of frustrated interactions in a Kuromoto model with inertia [37]. This Kuramoto model of phase oscillators can be mapped, in an approximate way, to a resistively coupled array of Josephson junctions [78]. Due to this connection, our first work on this important topic did involve Josephson junctions, and the generality of the phase approximation that is made in the Kuramoto model makes it of immediate relevance to the problem of achieving synchronicity in electrical power grids.

In Fig. 26 we show the time averaged order parameter as a function of the frustration and coupling strength K for a dilute network of Kuramoto–Sakaguchi oscillators with added inertia. The order parameter, which lies between 0 and 1, measures the degree of synchronicity in the network, with $r = 0$ corresponding to a completely desynchronized network in which each oscillator is oscillating independently. Here we have applied a random initial condition, adjacency matrix (controlling which oscillator is coupled to which) and distribution of natural frequencies for every pair of points in the (K, α)-plain, in order to ascertain the effect of increasing the frustration α. As we can see in the figure, there is a clearly defined region where it is possible to get partial synchronization despite having frustration in the network. In practice, this region is of importance as the reactance of the transmission lines in a real power grid produces phase differences which are well modeled by the frustration parameter(s) of this model.

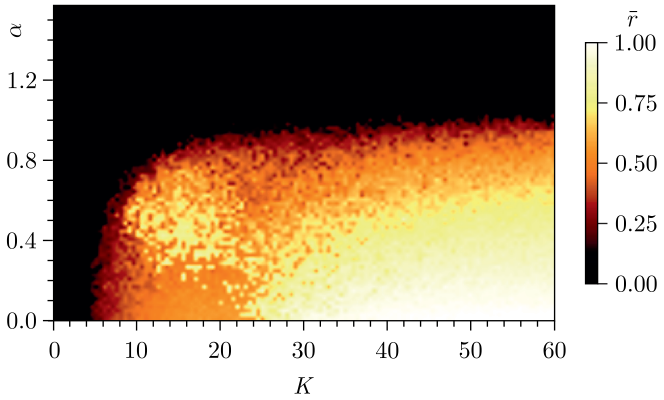

Fig. 26. Time-averaged order parameter, $\overline{r}$ over the (K, α)-plain with random initial conditions, coupling and natural frequencies. Here the dilution of each randomly coupled network was $p = 0.2$, and each network consisted of $N = 500$ oscillators. This means that there were $pN = 100$ nonzero elements in each adjacency matrix (consisting of zeros and ones) representing the random coupling. K is the coefficient of each adjacency matrix and α the frustration or phase-lag in the network. Adapted from [37]

In an attempt to improve the stability of synchrony in the so-called "smart" grids, several studies have attempted to incorporate different forms of control. In our recent work on power grids we have proposed using an improved form of control that minimizes losses in comparison to a nonlinear dissipative control scheme that was recently proposed by Arinushkin and Vadivasova [79]. Instead of applying the nonlinear damping to all the elements in the systems, we apply it only the arbitrarily chosen 5th element, i.e., $D_j = D_{0j}$ if $j \neq 5$ and $D_j = D_{0j} + k|\dot{\delta}_j|$ if $j = 5$. Here D_{0j} is the linear damping constant and k is the nonlinear damping constant. As we can see in Fig. 27, the addition of k causes a large improvement in the synchronicity of the grid. Comparison of the results given in Fig. 27, with those in Fig. 4 of [79], show that one can achieve the same degree of synchronicity in the grid by applying the nonlinear damping to any single element of the grid, as opposed to, to all of them, as was done in [79]. Paradoxically, the value of k required to achieve a certain degree of synchronicity in the case when nonlinear damping is applied only to one element is significantly smaller than when the nonlinear damping is applied to all the elements. This implies that the nonlinear control of one element can lead to a significant reduction in the dissipation that has to be added to the network as part of the control scheme, meaning that it would be much more efficient. Further details of our proposed control scheme have been published in collaboration with an M.Sc. student who is currently still participating in this activity [38].

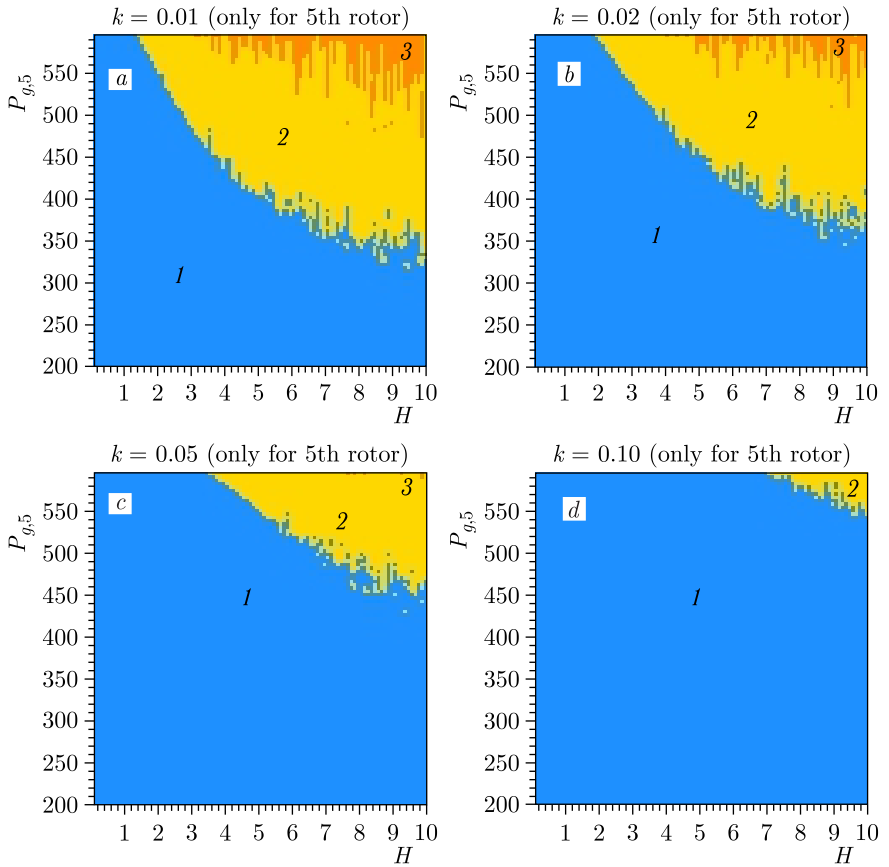

Fig. 27. Regime maps of the network of nonlinear oscillators discussed in [79], showing the effect of increasing the nonlinear damping coefficient k, for only the 5th rotor: $k = 0.01$ (a), $k = 0.02$ (b), $k = 0.05$ (c), $k = 0.10$ (d). Here H is the inertia parameter (the same for each rotor) and the output power of the 5th generator is $P_{g,5}$, with: *1* — area of the synchronous mode (blue); *2* — area of bi-stability (yellow); *3* — area of asynchronous behavior of one or more oscillators (orange). Adapted from Fig. 4 of [38]

19. CONCLUSION AND FUTURE OUTLOOK

Since 2011, we have cooperated on joint research involving theoretical and computational studies of Josephson nanostructures, with particular focus on the various nonlinear dynamic effects that are important in the variety of existing models for coupled Josephson junctions. Our collaboration has made it possible to simulate their phase dynamics, current–voltage characteristics, as well as several useful measures for the detection and analysis of chaos; such as, the Lyapunov exponent spectrum, Poncaré section, recurrence plot, etc.

We also appreciate that many of these results have required extensive computational time — representing, in totality, several hundreds of CPU years! — and would thus not have been possible without the excellent high-performance computation (HPC) support provided by the JINR and UNISA. During our collaboration over the past twelve years, we have also had to travel frequently between Russia and South Africa, especially during the pre-pandemic era, before it became easier to interact electronically via many meeting platforms that are now available. Thankfully, there were always opportunities, such as symposiums and conferences, and specific mobility funding to make these collaborative research visits possible. We note that on September 12, 2022, the 21st meeting of the Joint Coordination Committee (JCC) on cooperation between the Republic of South Africa and the Joint Institute for Nuclear Research was held in Cape Town (Fig. 28). Thus, in our view, our collaboration has flourished principly as a result of three favorable circumstances: (i) the realization of our common research interests and shared expertise in different areas, (ii) the availability of excellent computational facilities, and (iii) the ability to transcend boarders through air-travel and (more recently) online meeting platforms. As a result, our collaboration has been very productive. By involving the whole group at JINR (see Fig. 29), we have been able to relate many important physical aspects to the dynamics of systems of Josephson junctions. We have also made a significant contribution to gaining a better understanding of the multi-faceted, complex role played by chaos, synchronization, and other fascinating nonlinear effects, in structures composed of coupled Josephson junctions; whether they are coupled intrinsically, due to shunting, or as a result of incorporating the ferromagnetic materials that make it possible to control the magnetic properties via the superconducting current, and *vice versa*.

Fig. 28. On September 12, 2022, the 21st meeting of the Joint Coordination Committee (JCC) on cooperation between the Republic of South Africa and the Joint Institute for Nuclear Research was held in Cape Town

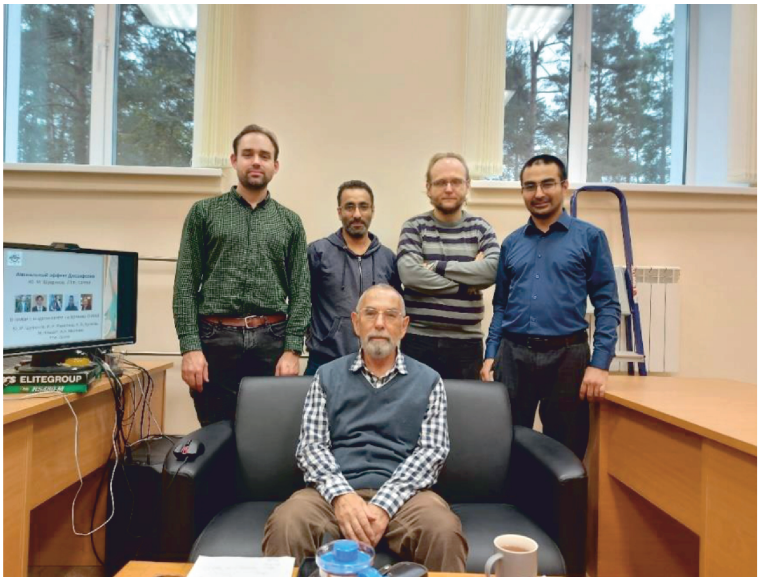

Fig. 29. The JINR group currently studying Josephson nanostructures

Today, superconductor electronics and spintronics based on Josephson nanostructures are intensively developing areas of condensed matter physics [46, 57, 80, 81]. An important part of this development is the study of Josephson junctions (JJs) that are coupled to magnetic systems. The ability to control the magnetic properties using the Josephson current, as well as the influence exerted on the superconducting current by the precession of the magnetic moment, attracts a great deal of attention.

Our main goal for our future collaboration is to create a base for fundamental and applied research in the field of superconducting electronics and spintronics in both countries. Currently, intensive joint work is being carried out on the simulation of superconducting nanostructures, in particular, coupled Josephson junctions, shunted systems, and hybrid Josephson structures with various types of barriers. This makes it possible to study the phase dynamics and current–voltage characteristics to obtain new information about various resonant and synchronization phenomena that influence the physical behavior of these structures. Such behavior includes, for example, switching, which is of importance to cryogenic memory.

REFERENCES

1. *Botha A. E., Qi G.* Optimised Periodic and Hyperchaotic Modes of a Triple Pendulum // Proc. of the 56th Ann. Conf. of the South African Inst. Phys., Pretoria, South Africa, July 12–15, 2011. P. 758–765.

2. *Shukrinov Yu.* Parametric Resonance Features in the Coupled Josephson Junctions // Book of Abstr. 56th Ann. Conf. of the South African Inst. of Phys., Pretoria, South Africa, July 12–15, 2011. P. 243–244.
3. *Shukrinov Yu. M., Hamdipour M., Kolahchi M. R., Botha A. E., Suzuki M.* Manifestation of Resonance-Related Chaos in Coupled Josephson Junctions // Phys. Lett. A. 2012. V. 376, No. 47. P. 3609–3619.
4. *Botha A. E., Shukrinov Yu. M., Kolahchi M. R.* Breathing Chimeras in a Stack of Intrinsically Coupled Josephson Junctions // Proc. of the 4th South Africa – JINR Symp. "Few to Many Body Systems", Dubna, Sept. 21–25, 2015. P. 135–141.
5. *Kolahchi M. R., Botha A. E., Shukrinov Yu. M.* Chimera States in an Intrinsically Coupled Stack of Josephson Junctions // J. Supercond. Nov. Magn. V. 30. P. 1659–1663.
6. *Benecha E. M., Dawood R., Rahmonov I. R., Shukrinov Yu. M., Botha A. E.* Simulations of dc SQUIDs with Topologically Trivial and Nontrivial Barriers // Proc. of the 4th South Africa – JINR Symp. "Few to Many Body Systems", Dubna, Sept. 21–25, 2015. P. 149–154.
7. *Shukrinov Yu. M., Medvedeva S. Yu., Botha A. E., Kolahchi M. R., Irie A.* Devil's Staircases and Continued Fractions in Josephson Junctions // Phys. Rev. B. 2013. V. 88. P 214515.
8. *Botha A. E., Shukrinov Yu. M., Kolahchi M. R.* Onset of Chaos in Intrinsic Josephson Junctions // Chaos, Solitons & Fractals, 2013. V. 48. P. 32–37.
9. *Kolahchi M. R., Shukrinov Yu. M., Hamdipour M., Botha A. E., Suzuki M.* Some Chaotic Features of Intrinsically Coupled Josephson Junctions // Physica C. 2013. V. 491. P. 63–65.
10. *Shukrinov Yu. M., Botha A. E., Medvedeva S. Yu., Kolahchi M. R., Irie A.* Structured Chaos in a Devil's Staircase of the Josephson Junction // Chaos. 2014. V. 24, No. 3. P. 033115.
11. *Shukrinov Yu. M., Azemtsa-Donfack H., Botha, A. E.* Chaos Induced by Coupling Between Josephson Junctions // JETP. Lett. 2015. V. 101. P. 251–257.
12. *Botha A. E., Shukrinov Yu. M., Medvedeva S. Yu., Kolahchi M. R.* Structured Chaos in 1-D Stacks of Intrinsic Josephson Junctions Irradiated by Electromagnetic Waves // J. Supercond. Nov. Magn. 2015. V. 28. P. 349–354.
13. *Yu. M. Shukrinov Yu. M., Rahmonov I. R., Kulikov K. V., Seidel P.* Effects of LC Shunting on the Shapiro Steps Features of Josephson Junction // Europhys. Lett. 2015. V. 110, No. 4. P. 47001.
14. *Shukrinov Yu. M., Azemtsa-Donfack H., Rahmonov I. R., Botha A. E.* Cascade of Parametric Resonances in Coupled Josephson Junctions // Low Temp. Phys. 2016. V. 42. P. 446–452.
15. *Botha A. E., Shukrinov Yu. M., Kolahchi M. R.* A Farey Staircase from the Two-Extremum Return Map of a JOsephson Junction // Nonlin. Dyn. 2016. V. 84. P. 1363–1372.
16. *Sokolović, I., Mali P., Odavić J., Radošević S., Medvedeva S.Yu., Botha A.E., Shukrinov Yu. M., Tekić J.* Devil's staircase and the absence of chaos in the dc- and ac-driven overdamped Frenkel-Kontorova model // Phys. Rev. E. 2017. V. 96. P. 022210.
17. *Shukrinov Yu. M., Rahmonov I. R., Kulikov K. V., Botha A. E., Plecenik A., Seidel P., Nawrocki W.* Modeling of LC-Shunted Intrinsic Josephson Junctions in High-T c Superconductors // Supercond. Science Techn. 2017. V. 30, No. 2. P. 024006.

18. *Nashaat M., Botha A. E., Shukrinov Yu. M.* Devil's Staircases in the IV Characteristics of Superconductor/Ferromagnet/Superconductor Josephson Junctions // Phys. Rev. B. 2018. V. 97. P. 224514.
19. *Botha A. E., Rahmonov I. R., Shukrinov Yu. M.* Spontaneous and Controlled Chaos Synchronization in Intrinsic Josephson Junctions // IEEE Trans. Appl. Supercond. 2018. V. 28, No. 7. P. 1800806.
20. *Shukrinov Yu. M., Mazanik A., Rahmonov I. R., Botha A. E., Buzdin A* Re-Orientation of the Easy Axis in φ_0-Junction // Europhys. Lett. 2018. V. 122, No. 3. P. 37001.
21. *Shukrinov Yu. M., Rahmonov I. R., Botha A. E.* Superconducting Spintronics in the Presence of Spin-Orbital Coupling // IEEE Trans. Appl.Supercond. 2018. V. 28, No. 7. P. 1800505.
22. *Tekić, J., Botha A. E., Mali P., Shukrinov Yu. M.* Inertial Effects in the dc + ac Driven Underdamped Frenkel–Kontorova Model: Subharmonic Steps, Chaos, and Hysteresis // Phys. Rev. E. 2019. V. 99. P. 022206.
23. *Benecha M., Rahmonov I. R., Shukrinov Yu. M., Botha A. E., Ananikian N.* Modeling of dc SQUIDs With Topologically Nontrivial Barriers // Arm. J. Phys. 2019. V. 12. P. 226–232.
24. *Mazanik A. A., Rahmonov I. R., Botha A. E., Shukrinov Yu. M.* Analytical Criteria for Magnetization Reversal in a φ_0 Josephson Junction // Phys. Rev. Appl. 2020. V. 14. P. 014003.
25. *Shukrinov Yu. M., Rahmonov I. R., Botha A. E.* Peculiarities of IV-Characteristics and Magnetization Dynamics in the φ_0 Josephson Junction // Low Temp. Phys. 2020. V. 46, No. 9. P. 932–938.
26. *Tekić J., Botha A. E., Mali P., Shukrinov Yu. M.* The AC Driven Frenkel–Kontorova Model: From Shapiro Steps to Chaos // 13th Chaotic Modeling and Simulation Intern. Conf. 2021. Cham: Springer Intern. Publ., P. 943–951.
27. *Shukrinov Yu. M., Abouhaswa A. S., Botha A. E.* Double and Triple Resonance Behaviour in Large Systems of LC-Shunted Intrinsic Josephson Junctions // Phys. Lett. A. 2021. V. 387. P. 127025.
28. *Botha A. E., Shukrinov Yu. M., Tekić J.* Chaos Along the rc-Branch of RLC-Shunted Intrinsic Josephson Junctions // Chaos, Solitons & Fractals. 2022. V. 156. P. 111865.
29. *Nashaat M., Sameh M., Botha A. E., Kulikov K. V., Shukrinov Yu. M.* Bifurcation Structure and Chaos in Dynamics of Nanomagnet Coupled to Josephson Junction // Chaos. 2022. V. 32, No. 9. P. 093142.
30. *Mazanik A. A., Botha A. E., Rahmonov I. R., Shukrinov Yu. M.* Hysteresis and Chaos in Anomalous Josephson Junctions Without Capacitance. 2023. arXiv:2311.00597.
31. *Botha A. E., Shukrinov Yu. M., Tekić, J., Kolahchi M. R.* Chaotic Dynamics from Coupled Magnetic Monodomain and Josephson Current // Phys. Rev. E. 2023. V. 107. P. 024205.
32. *Botha A. E., Shukrinov Yu. M.* Observation of Chaotic Behaviour in the CCJJ + DC Model of Coupled Josephson Junctions // Chaotic Modeling Simulation. 2013. V. 2. P. 265–272.
33. *Azemtsa-Donfack H., Shukrinov Yu. M., Rahmonov I. R.* Can Shapiro Step Subharmonics be "Charged"? // Proc. of the 59th Ann. Conf. of the South African Inst. Phys. SAIP2014, Univ. of Johannesburg, 2015. P. 22–28.
34. *Shukrinov Yu. M., Rahmonov I. R., Kulikov K. V., Botha A. E., Gaafar M., El Samman H., Dawood R., Nashaat M., El Sherbini T.* Intrinsic Josephson Junctions for Superconducting Electronics and Quantum Computation // Proc.

of the 15th Intern. Supercond. Electronics Conf. (ISEC 2015), Japan, July, 6–9. 2015. P. DP-P02.
35. *Botha A. E., Shukrinov Yu. M., Rahmonov I. R., Kulikov K. V., Kolahchi M. R.* Synchronization and Chaos Control Features in Arrays of Intrinsic Josephson Junctions // 16th Intern. Supercond. Electronics Conf. (ISEC), Naples, Italy, June 12–16, 2017. IEEE Xplore, 2017. P. 1–4.
36. *Shukrinov Yu. M., Rahmonov I. R., Botha A. E.* Dynamics of Anomalous Josephson Effect in Superconducting Nanostructures // AIP Conf. Proc. 2022. V. 2551, No. 1. P. 020003.
37. *Botha A. E., Eclerová V., Shukrinov Yu. M., Kolahchi M. R.* Effects of Frustrated Interactions on Synchronicity in Electrical Power Grids // 15th Chaotic Modeling and Simulation Intern. Conf. Cham: Springer Intern. Publ., 2023. P. 53–61.
38. *Olivier C., Shukrinov Yu. M., Botha A. E.* Evaluation of Proportional and Nonlinear Damping Control Schemes in an Optimized Power Grid // Intern. Conf. on Electrical, Comput. and Energy Technol. (ICECET'2023). 2023. P. 1–6.
39. *Kolahchi M. R., Shukrinov Yu. M., Botha A. E.* Resonance Overlap as the Origin of Structured Chaos in Josephson Junctions // Book of Abstr. of the 9th Intern. Symp. on Intrinsic Josephson Effects and THz Plasma Oscillations in High-Tc Superconductors (THz-PLASMA 2014), Kyoto, Japan, Nov. 30 – Dec. 3, Kyoto Univ., 2014. P. 22.
40. *Shukrinov Yu. M., Rahmonov I. R., Kulikov K. V., Botha A. E., Sengupta K., Seidel P.* Modelling of Josephson Nanostructures // Proc. of XXI Symp. "Nanophysics and Nanoelectronics", Nizhniy Novgorod, March 13–16, 2017. Publ. house of Nizhniy Novgorod State Univ. 2017. V. 1. P. 122–123.
41. *Shukrinov Yu., Rahmonov I., Botha A. E., Plecenik A., Angel D.* Magnetization Dynamics Features in the SFS φ_0 Josephson Junction // Intern.l Conf. on UK–China Emerging Technol. (UCET'2020), Glasgow, UK, Aug. 20–21, 2020. IEEE Xplore, 2020. P. 1–2.
42. *Nashaat M., Sameh M., Botha A. E., Kulikov K. V., Shukrinov Yu. M.* Bifurcations in Josephson Junction Coupled to the Nanomagnet // Proc. of XXVI Symp. "Nanophysics and Nanoelectronics", Nizhnii Novgorod, March 14–17, 2022. Publ. house of Nizhniy Novgorod State Univ., 2022. V. 1. P. 17–18.
43. *Shukrinov Yu. M., Rahmonov I. R., Kulikov K. V., Abdelmoneim S. A., Nashaat M., Janalizadeh A., Kolahchi M. R., Botha A. E., Tekić J.* Nonlinearity, Locking, and Chaos in Anomalous Josephson Junctions // Proc. of XXVII Symp. "Nanophysics and Nanoelectronics", Nizhnii Novgorod, March 13–16, 2023. Publ. house of Nizhniy Novgorod State Univ., 2023. V. 1. P. 132–133.
44. *Tsujimoto M., Yamamoto T., Delfanazari K., Nakayama R., Kitamura T., Sawamura M., Kashiwagi T., Minami H., Tachiki M., Kadowaki K., Klemm R. A.* Broadly Tunable Subterahertz Emission from Internal Branches of the Current-Voltage Characteristics of Superconducting $Bi_2Sr_2CaCu_2O_{8+\delta}$ Single Crystals // Phys. Rev. Lett., 2012. V. 108. P. 107006.
45. *Yao Y., Cai R., Yang S. H., Xing W., Ma Y., Mori M., Ji Y., Maekawa S., Xie X. C., Han W.* Half-Integer Shapiro Steps in Strong Ferromagnetic Josephson Junctions // Phys. Rev. B. 2021. V. 104. P. 104414.
46. *Shukrinov Yu. M.* Anomalous Josephson Effect // Phys. Usp. 2022. V. 65. P. 317–354.
47. *Linder J., Halterman K.* Superconducting Spintronics with Magnetic Domain Walls // Phys. Rev. B. 2014. V. 90. P. 104502.

48. *Shukrinov Yu. M., Rahmonov I. R., Sengupta K., Buzdin A.* Magnetization Reversal by Superconducting Current in φ_0 Josephson Junctions // Appl. Phys. Lett. 2017. V. 110, No. 18. P. 182407.
49. *Buzdin A. I.* Proximity Effects in Superconductor–Ferromagnet Heterostructures // Rev. Mod. Phys. 2005. V. 77. P. 935–976.
50. *Buzdin A.* Direct Coupling Between Magnetism and Superconducting Current in the Josephson φ_0 Junction // Phys. Rev. Lett. 2008. V. 101. P. 10700.
51. *Golubov A. A., Kupriyanov M. Yu., Il'ichev E.* The Current-Phase Relation in Josephson Junctions // Rev. Mod. Phys. 2004. V. 76. P. 411–469.
52. *Bergeret F. S., Volkov A. F., Efetov K. B.* Odd Triplet Superconductivity and Related Phenomena in Superconductor–Ferromagnet Structures // Rev. Mod. Phys. 2005. V. 77. P. 1321–1373.
53. *Kuramoto Y., Battogtokh D.* Coexistence of Coherence and Incoherence in Nonlocally Coupled Phase Oscillators // Nonlin. Phenom. Complex Syst. 2002. V. 5. P. 380–385.
54. *Abrams D. M., Strogatz S. H.* Chimera States for Coupled Oscillators // Phys. Rev. Lett. 2004. V. 93. P. 174102.
55. *Shukrinov Yu. M., Mahfouzi F., Seidel P.* Equidistance of Branch Structure in Capacitively Coupled Josephson Junctions Model with Diffusion Current // Phys. C. 2006. V. 449, No. 1. P. 62–66.
56. *Shukrinov Yu. M., Rahmonov I. R., Gaafar M. A.* Calculation of the Plasma Frequency of a Stack of Coupled Josephson Junctions Irradiated with Electromagnetic Waves // Phys. Rev. B. 2012. V. 86. P. 184502.
57. *Linder J., Robinson J. W. A.* Superconducting Spintronics // Nature Phys. 2015. V. 11, No. 4. P. 307–315.
58. *Kapitza P. L.* Pendulum with a Vibrating Suspension // Usp. Fiz. Nauk. 1951. V. 44. P. 7–15.
59. *Marin Bukov L. D., Polkovnikov A.* Universal High–Frequency Behavior of Periodically Driven Systems: From Dynamical Stabilization to Floquet Engineering // Adv. Phys. 2015. V. 64. P. 139–226.
60. *Borromeo M., Marchesoni F.* Artificial Sieves for Quasimassless Particles // Phys. Rev. Lett. 2007. V. 99. P. 150605.
61. *Aidelsburger M., Lohse M., Schweizer C. et al.* Measuring the Chern Number of Hofstadter Bands with Ultracold Bosonic Atoms // Nature Phys. 2015. V. 11. P. 162–166.
62. *Wickenbrock A., Holz P. C., Wahab N. A., Abdul, Phoonthong P., Cubero D., Renzoni F.* Vibrational Mechanics in an Optical Lattice: Controlling Transport via Potential Renormalization // Phys. Rev. Lett. 2012. V. 108. P. 020603.
63. *Chizhevsky V. N.* Experimental Evidence of Vibrational Resonance in a Multistable System // Phys. Rev. E. 2014. V. 89. P. 062914.
64. *Uzuntarla M., Yilmaz E., Wagemakers A., Ozer M.* Vibrational Resonance in a Heterogeneous Scale Free Network of Neurons // Commun. Nonlin. Science Numer. Simulation. 2015. V. 22, No. 1. P. 367–374.
65. *Boukobza E., Moore M. G., Cohen D. Vardi A.* Nonlinear Phase Dynamics in a Driven Bosonic Josephson Junction // Phys. Rev. Lett. 2010. V. 104, No. 24. P. 240402.
66. *Citro R., Torre E. G. D., D'Alessiod L., Polkovnikov A., Babadi M., Oka T., Demler E.* Dynamical Stability of a Many-Body Kapitza Pendulum // Ann. Phys. 2015. V. 360. P. 694.

67. *Fialko O., Opanchuk B., Sidorov A. I., Drummond P. D., Brand J.* Fate of the False Vacuum: Towards Realization with Ultra-Cold Atoms // Europhys. Lett. 2015. V. 110, No. 5. P. 56001.
68. *Longhi S.* Rapidly Oscillating Scatteringless Non-Hermitian Potentials and the Absence of Kapitza Stabilization // Europhys. Lett. 2017. V. 118, No. 2. P. 20004.
69. *Shayak B.* A Mechanism for Electromagnetic Trapping of Extended Objects // Europhys. Lett. 2017. V. 118, No. 4. P. 45002.
70. *Martin J., Georgeot B., Guéry-Odelin D., Shepelyansky D. L.* Kapitza Stabilization of a Repulsive Bose–Einstein Condensate in an Oscillating Optical Lattice // Phys. Rev. A. 2018. V. 97. P. 023607.
71. *Shukrinov Yu. M., Nashaat M., Rahmonova I. R., Kulikov K. V.* Ferromagnetic Resonance and the Dynamics of the Magnetic Moment in a Josephson Junction–Nanomagnet System // JETP Lett. 2019. V. 110, No. 3. P. 160–165.
72. *Motter A. E., Myers S. A., Anghel M., Nishikawa T.* Spontaneous Synchrony in Power-Grid Networks // Nat. Phys. 2013. V. 9. P. 191.
73. *Auer S., Hellmann F., Krause M., Kurths J.* Stability of Synchrony Against Local Intermittent Fluctuations in Tree-Like Power Grids // Chaos. 2017. V. 27. P. 127003.
74. *Schäfer B., Yalcin G. C.* Dynamical Modeling of Cascading Failures in the Turkish Power Grid // Chaos. 2019. V. 29. P. 093134.
75. *Anvari M. et al.* Short Term Fluctuations of Wind and Solar Power Systems // New J. Phys. 2016. V. 18. P. 063027.
76. *Coetzee D., Els M.* The Impact Of Load Shedding On The Construction Industry In South Africa // Emerging Trends in Construction Organisational Practices and Project Management Knowledge Areas. Cape Town: Univ. of Cape Town, 2016. P. 268.
77. *Himansu Das, Gouri Sankar Panda, Bhagaban Muduli, Pradeep Kumar Rath* The Complex Network Analysis of Power Grid: A Case Study of the West Bengal Power Network // Intelligent Comput., Networking, Informatics. New Delhi, 2014. P. 17–29.
78. *Wiesenfeld K., Colet P., Strogatz S. H.* Synchronization Transitions in a Disordered Josephson Series Array // Phys. Rev. Lett. 1996. V. 76. P. 404–407.
79. *Arinushkin P. A., Vadivasova T. E.* Nonlinear Damping Effects in a Simplified Power Grid Model Based on Coupled Kuramoto-Like Oscillators with Inertia // Chaos, Solitons and Fractals. 2021. V. 152. P. 111343.
80. *Mel'nikov A. S., Mironov S. V., Samokhvalov A. V., Buzdin A. I.* Superconducting Spintronics: State of the Art and Prospects // Phys. Usp. 2022. V. 65, No. 12. P. 1248–1289.
81. *Bobkova I. V., Bobkov A. M., Silaev M. A.* Magnetoelectric Effects in Josephson Junctions // J. Phys.: Conden. Matter. 2022. V. 34. P. 353001.

Received on March 29, 2024.

Редактор *Е. И. Крупко*

Подписано в печать 08.04.2024.
Формат 60 × 90/16. Бумага офсетная. Печать цифровая.
Усл. печ. л. 1,25. Уч.-изд. л. 1,14. Тираж 110 экз. Заказ № 60846.

Издательский отдел Объединенного института ядерных исследований
141980, г. Дубна, Московская обл., ул. Жолио-Кюри, 6.
E-mail: publish@jinr.ru
www.jinr.ru/publish/